Study on Energy Recovery and Anhydrite Production from Elemental Sulfur

by

Yasmine M. Hajar

A thesis submitted to the Department of Chemical Engineering

In conformity with the requirements for

the degree of Master of Applied Science

Queen's University

Kingston, Ontario, Canada

August, 2015

Abstract

An industrial-scale model was developed for production of anhydrite ($CaSO_4$) via oxidation of elemental sulfur (S) with calcite ($CaCO_3$), and potential electrical generation. In the proposed system, sulfur is first oxidized in a combustion chamber to form sulfur dioxide (SO_2) at high temperature and pressure, and expanded in a turbine to produce electrical power. Then, the SO_2 is converted to $CaSO_4$ through a Flue Gas Desulfurization (FGD) boiler. Further energy is recovered from the flue gas through a Heat Recovery Steam Generator (HRSG). In this study, three cases were elaborated, with the best resulting in a predicted power production of 531 MW from a flow of sulfur at 72 kg/s. The corresponding CO_2 emissions are 0.675 kg/kWh, less than a new coal-fired plant's emissions of 0.762 kg/kWh.

Experimental studies were undertaken to test for the sulfur conversion to anhydrite in two different lab-scale reactor systems. In the first, sulfur was gasified in an evaporator, and the resulting gas was flowed to a reactor containing calcite, similarly to a FGD system. In the second, sulfur and calcite were inserted in the same vessel to test for direct reaction. Using thermogravimetric and x-ray diffraction tests, it was found that the sulfation percentage increased as a function of temperature from 600 to 800 ^{0}C, and was close in value at 800 and 900 ^{0}C. The increase of temperature resulted in calcination of calcite to lime (CaO), which reacts better with sulfur; however, when reaching 900 ^{0}C, sintering may have occurred, resulting in obstruction of further conversion. Molar ratios of S-$CaCO_3$ of 0.5 showed a better conversion of sulfur (at 700, 800 and 900 ^{0}C) than when the reactants were equimolar. Using pure oxygen instead of air almost always showed a higher conversion for all temperatures and reactant ratios.

Acknowledgements

Above all, I would like to express my gratitude to my supervisors Dr. Frank Zeman and Dr. Kim McAuley, for their guidance, advice and encouragement throughout my research work. It was a great experience, and a pleasure to work in such a great environment, both at Queen's university and Royal Military College.

I would also like to thank Clarence McEwen, Brent Ball and Tim Nash for their technical support in designing the apparatus. Many thanks to Dr. Jennifer Snelgrove for her help in using the Thermogravimetric apparatus and a great appreciation to Bob Whitehead and Agatha Dobosz for their assistance in x-ray testing.

Many thanks also to the faculty, staff and students of the Department of Chemical Engineering at Queen's and RMC, who made my time in the past two years very enjoyable.

Finally, I would like to thank my mother for her great support throughout the years and for always pushing me to set my goals higher; a greater gratitude for my father whom I have always looked up for, in his wisdom in life and love of knowledge. Not forgetting my younger sister and brother for being themselves and there for me at all times.

Table of Contents

List of Figures

List of Tables

List of Abbreviations

Acronyms	
API	American Petroleum Institute
$CaCO_3$	Calcium Carbonate/ Calcite
CaO	Calcium oxide/ Quick Lime
$Ca(OH)_2$	Calcium hydroxide/ Hydrated or Slaked Lime/ Portlandite
$CaSO_4$	Anhydrite/ Calcium Sulfate
$CaSO_4.2H_2O$	Gypsum
COT	Combustor Outlet Temperature
DAQ	Data Acquisition
EDS	Energy Dispersive X-ray Spectroscopy
FBC	Fluidized Bed Combustor
FGD	Flue Gas Desulfurization
GHG	Greenhouse Gas
HDS	Hydrodesulfurization
HP	High Pressure
HRSG	Heat Recovery Steam Generator
H_2S	Hydrogen Sulfide
H_2SO_4	Sulfuric Acid
IP	Intermediate Pressure
LHV	Low Heating Value
LIMB	Lime Injection Multistage Burner
LP	Low Pressure
LSD	Lime Spray Drying
NGCC	Natural Gas Combined Cycle
NI	National Instrument
PC	Pulverized Coal
PID	Proportional, Integral and Derivative
SCC	Sulfur Combined Cycle
SEM	Scanning Electron Microscopy
SO_2	Sulfur Dioxide
TA	Thermal Analysis
TGA	Thermogravimetric Analysis
TIT	Turbine Inlet Temperature
TOT	Turbine Outlet Temperature
USB	Universal Serial Bus
XRD	X-Ray Diffraction

Symbols

Å	Angstrom
kV	Kilovolt
mA	Milliampere
MT	Million Metric Tonnes
µm	Micrometer
C_p	Specific Heat (J/mol.K)
h	Enthalpy
ΔH^0	Standard Enthalpy Change (J/mol)
$\Delta \dot{H}^0$	Standard Enthalpy Change Rate (W)
$\dot{m}$	Mass Flow (kg/s)
Mt	Million tonne
η	Efficiency
$\dot{n}$	Molar Flow (mol/s)
θ	Angle Theta (rad)
P	Pressure (bar)
$\dot{Q}$	Heat Input Rate (W)
R	Ideal Gas Constant (J/mol.K)
T	Temperature (^{0}C)
v	Coefficients of Reactions
$\dot{W}$	Work Rate or Power (W)
x	Fraction

Subscripts

CC	Combustion Chamber
comb	Combustion
comp	Compressor
f	Formation
HP	High Pressure
HRSG	Heat Recovery Steam Generator
i	Species
ig	Ideal gas
IP	Intermediate Pressure
k	Stream number
l	Liquid
LP	Low Pressure
m	Melting
S	Sulfur
s	Solid
steam	Steam in the HRSG
th	Thermal
turb	Turbine
u	Operating unit
w	Water

To the Future and All Its Unveiled Chapters,

Chapter 1

Introduction

"Old woman, bring some sulfur, and make some fire, so I can purge the hall from this pollution" Homer: the Odyssey- Book XXII.

One of the oldest written references for sulfur in human history, this pure material known as Brimstone or burning stone was believed to have great divine power and therefore was used as medicine, fumigant and incense in religious rites to purify air from evil spirits [1]. From the volcanic soils of Sicily to the Yangmingchan National Park in Taiwan, elemental sulfur was mined and traded throughout the world. When Europeans learned about the gunpowder abilities of sulfur, they increased sulfur mining and started looking for more sources of sulfur. In the late 1800s, with the increased use of sulfur, especially in its sulfuric acid form, the Frasch method was invented in the USA to remove sulfur from underground salt domes [2].

Sulfur also exists in nature combined with other elements such as copper, iron and lead. When combined with calcium, the mineral formed is gypsum ($CaSO_4.2H_2O$), a hydrated form of anhydrite ($CaSO_4$). Gypsum is widely available in the Earth's crust and is extensively mined. It is mostly used as a construction material to make plaster, Portland cement and wallboard [3]. Currently, gypsum from industrial sources, known as "synthetic" gypsum, is also being produced at an increasing rate. Synthetic gypsum is primarily the by-product of flue gas desulfurization (FGD) processes in coal-fired power plants where Sulfur Dioxide (SO_2) is converted to gypsum to prevent acid rains, in a post-combustion process [4]. Sulfur is also removed from petroleum products to prevent SO_2 emissions during combustion. Sulfur removal from gaseous and liquid

hydrocarbons in petroleum industries, is a pre-combustion process where hydrocarbons are scrubbed with hydrogen to remove sulfur as hydrogen sulfide (H_2S) [5]. Sulfur in natural gas is present as H_2S; therefore, there is no need for hydrogen scrubbing. Once H_2S is separated, it can be converted to elemental sulfur (S) through the "Claus process" [5]. Sulfur removal has increased substantially in the past decade because of the more restricted diesel regulations and the low percentage of sulfur allowed in fuels [6]. As a result of the regulations for sweetening treatment, sulfur recovery from natural gas and petroleum products became the world's leading supply source since the 1980s, replacing mining [6]. Canada is the second largest producer of by-product sulfur after the USA, and the world's largest exporter, selling sulfur to about twenty countries [7]. 90 % of sulfur consumption is as sulfuric acid (H_2SO_4) and most of it is used for leaching processes [8]. In Canada, the amounts of sulfur recovered are larger than its demand, resulting in a surplus of the material and an inventory of 12.3 Mt in 2009. 8 Mt of the inventory belong to Syncrude Canada Ltd in Fort McMurray, Alberta.

Stockpiling sulfur in its elemental form is hazardous because of the high risks of oxidation and fire, and the formation of the corrosive sulfuric acid when reacted with water. Therefore, sulfur storage has to be replaced by a process that converts sulfur from a noxious reactive compound to a thermodynamically stable form. The proposed pathway is to convert waste sulfur into its natural form anhydrite ($CaSO_4$), which if hydrated, becomes gypsum ($CaSO_4.2H_2O$), an environmentally benign form.

$$CaCO_3(s) + S(s) + 3/2\, O_2(g) \rightarrow CaSO_4(s) + CO_2(g) \qquad \Delta H^0 = -620.4\ kJ/mol \qquad \text{(R1.1)}$$

1.1 Summary of Chapters Content

In Chapter 2, background concerning sulfur life cycle is provided; along with literature review about mobilization of sulfur in oil refineries. Literature about FGD systems was also necessary to be shown as it makes the basis for the thermodynamic study in Chapter 3 and the experimental design in Chapter 4.

Chapter 3 is a preliminary study of a potential large-scale process to convert sulfur to gypsum while recovering energy to produce electricity; this study had a purpose of making the process appealing for integration into refineries or other chemical processing plants, (e.g., cement kilns).

Chapter 4 describes the design of a lab-scale process for reacting sulfur with calcite to produce calcium sulfate. This process was different from FGD experiments in literature by the fact that the starting material is elemental sulfur instead of SO_2. The effects of temperature, gas used and reactant ratio, in different designed systems was studied.

Chapter 5 summarizes the conclusions and provides recommendations for future work.

1.1 References for Chapter 1

[1] Prud'Homme M. Sulphur. The Canadian Encyclopedia. Toronto: Historica Canada. (2006).

[2] Apodaca LE. Sulfur. Mineral Commodity Summaries 2015. (2015) 156-157.

[3] Olson DW. Gypsum. U.S. Geological Survey (2001).

[4] Srivastava RK. Flue gas desulfurization; the state of the art. Air and waste manage. 51 (2001) 1676-1688.

[5] M.P. Elsner, M. Menge, C. Müller, D.W. Agar, The Claus process: teaching an old dog new tricks, Catalysis Today. 79–80 (2003) 487-494.

[6] Environment Canada, Sulphur in Diesel Fuel Regulations. (2014).

[7] Canadian Minerals Yearbook (CMY) – 2009. Sulphur. Natural Resources Canada. (2009).

[8] Meyer B. Elemental sulfur. Chemical reviews. 76-3 (1976).

[9] Rappold TA, K.S. Lackner KS, Large scale disposal of waste sulfur: From sulfide fuels to sulfate sequestration, Energy. 35 (2010) 1368-1380.

Chapter 2

Literature Review

2.1 Life Cycle of Sulfur and Potential Large-Scale Disposal Approaches

The typical industrial life cycle of sulfur starts with extraction from a source and ends with its release to the environment, in a toxic or benign form. Lackner and Rappold affirm that it is important to choose pathways for "mobilizing" sulfur into well-controlled sinks with a low threat to the ecosystem [1]. Currently, more than 190 Mt/yr of sulfur are produced worldwide through industrial activities (i.e. coal, petroleum, metallurgy and mining), compared to the 35 Mt/yr mobilized naturally by environmental emissions [3]. The current industrial life cycle of sulfur ends with ~30 % of it emitted to the atmosphere (as SO_2), ~40 % escaping as fertilizers and wastes (in sulfate, SO_4^{2-} and sulfide, S^{2-} forms) and the rest being converted to gypsum or stockpiled in solid form [4]. Atmospheric emissions are concentrated more in the industrialized world than in developing countries [5]. Lackner and Rappold proposed a large scale disposal of sulfur, into natural reservoirs, in its stable sulfate form. Reducing sulfur into sulfuric acid then neutralizing it with common alkaline rocks would allow the formation of benign sulfates and thus ending the life cycle of sulfur. The sulfates formed, depending on the alkaline rock, can be soluble or insoluble in water. Magnesium, sodium and potassium sulfates are present in ocean at a mass of ~120 x 10^7 Mt, far exceeding the amount of sulfur mobilized through industry. Therefore, Rappold and Lackner proposed disposing sulfate as a soluble salt in the ocean.

Rather than treating sulfur as a waste, it could be treated as a source of fuel because of the high heating value stored in this compound. Sulfuric acid production and neutralization reactions are

exothermic and produce useful energy if recovered. H_2S conversion to sulfuric acid produces heat of a value higher than that of coal (793 kJ/mol compared to 500 kJ/mol) [1]. In addition, sulfuric acid neutralization further adds heat to the total heat recovered that varies in value depending on the alkali used for the neutralization. Lackner and Rappold have favored the use of olivine, or magnesium silicates (Mg_2SiO_4) for neutralization, but also suggested the use of carbonates (e.g., $CaCO_3$, $MgCO_3$ and $NaCO_3$). The downside consequence of the use of carbonates is the CO_2 production during the neutralization reaction. Carbonates, especially calcite ($CaCO_3$) are widely available in nature; therefore, they are commonly used in the neutralization of strong acids, despite the potential CO_2 emissions. Currently, 10 Mt of sulfur from coal combustion is converted to gypsum ($CaSO_4.2H_2O$) using calcite [2]. When sulfur is sequestered as gypsum, it can be used in cement, wallboard or fertilizers industries.

2.2 Sulfur Removal in Petroleum Refineries

Hydrodesulfurization (HDS) is the process of removing sulfur from sulfuric compounds (e.g., thiophenes, and benzothiophenes) when using hydrogen to form hydrogen sulfide (H_2S), in petroleum refineries [4]. Sulfur in light fuels such as natural gas, is present naturally in H_2S form resulting in no need of hydrogen scrubbing for natural gas to separate sulfur from the hydrocarbons. In heavy fuels, however, sulfuric compounds are present in various forms and vary in reactivity and strength of C-S bonds. The stronger the bond is, the more difficult it is to scrub out sulfur and reduce the amount left in crude oil. More extreme reaction conditions can be used but they might result in negative effect on the oil's final properties (e.g., octane number and API value) [4].

Sulfur removal from petroleum compounds is becoming more challenging due to concerns regarding acid rains; the maximum allowable sulfur content have dropped in value to 15 ppm, in Canada and many other countries [5]. Once sulfur is removed as hydrogen sulfide, it can be either injected underground or processed to elemental sulfur.

2.3 Claus Process, the Process Leading to Sulfur Stockpiling

Hydrogen sulfide (H_2S), produced as a by-product from crude oil and natural gas sweetening, is converted to elemental sulfur by the "Claus process". This process consists of two parts: a reactor furnace and multistage catalytic bed convertors [6]. In the furnace, one third of the H_2S is combusted with air to form SO_2 (R2.1). This reaction occurs at a temperature higher than 1000 ^{0}C and a gauge pressure around 70 kPa. Energy from the high temperature gas is recovered in a waste heat boiler to produce steam. Gases are cooled before entering the catalyst beds to prevent damage of the catalyst. The remaining unreacted H_2S reacts catalytically with SO_2 to produce sulfur and water (R2.2):

$$H_2S(g) + 3/2O_2(g) \rightleftharpoons SO_2(g) + H_2O(g) \qquad \Delta H^0 = -369.6\ kJ/mol \qquad \text{(R2.1)}$$

$$2H_2S(g) + SO_2(g) \rightleftharpoons 3/8S_8(g) + 2H_2O(g) \qquad \Delta H^0 = -108\ kJ/mol \qquad \text{(R2.2)}$$

Three catalytic beds in series are used to recover 95-97 % of the sulfur [6]. Gaseous sulfur is condensed and cooled to its solid state, and piled in large stockpiles as elemental sulfur (S).

2.4 Flue Gas Desulfurization Process Review and Analogy between SO_2 and S conversion to $CaSO_4$

The sulfur stockpiles at the petroleum refineries are causing environmental concerns at the long-term. The Claus process that converts H_2S to elemental sulfur should be replaced by a more

environmental process in which sulfur could be converted to a benign form that is at a thermodynamic ground-state. The suggested process in this thesis is to convert sulfur to anhydrite ($CaSO_4$) similarly to the Flue Gas Desulfurization (FGD) process used in coal plants, where SO_2 is converted to $CaSO_4$ or its hydrated form gypsum, $CaSO_4.2H_2O$.

2.4.1 Types of FGD Systems

In coal plants, there are many types of FGD systems that are used to scrub SO_2 from flue gas. They can be categorized as regenerative or non-regenerative systems. Regenerative FGD systems are cyclic processes where the absorbent (e.g., amine, activated carbon, sodium carbonate) is returned to the process after it reacts with SO_2, resulting in lower sorbent usage but more complex systems [7]. Non-regenerative systems are processes where sorbents such as natural limestone (containing calcite, $CaCO_3$) are used in a single pass stream. The downstream from the reaction with SO_2, results in either a saleable or a waste product depending on the purity of the anhydrite or gypsum. Non-regenerative processes are less complicated than the regenerative type and have lower operating costs, due to the non-recycling of the reacted sorbent.

Another way of classifying FGD systems is based on the state of the sorbent [8]. Thus, the system can be “wet” when a liquid or slurry sorbent is used or “dry” when the absorbing matter is in the solid-state.

In typical wet FGD systems, hydrated lime ($Ca(OH)_2$) slurry is sprayed from top of a tower to absorb SO_2. Wet FGD systems have the highest efficiency in capturing SO_2 and a low utility consumption because they run at low temperatures; but are more likely to produce hannebachite ($CaSO_3.0.5H_2O$) instead of saleable gypsum [8]. Dry and semi-dry processes have lower capital costs but higher operating costs because of the high temperatures required. An example of a semi-

dry FGD system is Lime Spray Drying (LSD) where slurry lime is injected from top of the tower and removed as anhydrite ($CaSO_4$) from the bottom, after reacting with SO_2 at high temperatures. The efficiency of the desulfurization in semi-dry processes is lower than that in wet scrubbers (a maximum of 70 % compared to ~90 % for wet processes); therefore, it is typically used for scrubbing flue gas from combustion of coal with less than 2 % sulfur content [7]. In dry FGD systems, such as Lime Injection Multistage Burners (LIMBs) or Fluidized Bed Combustors (FBCs), the limestone sorbent is injected into the boiler bed at temperatures above 800 ^{0}C [9]. The advantages of using dry and semi-dry technology are the formation of a dry product (anhydrite), the fewer corrosion problems due to the absence of water, and the no reheating or large space requirements. More importantly, the starting material used in dry FGD, which is natural limestone, is a much cheaper sorbent than the expensive hydrated lime, $Ca(OH)_2$.

2.4.2 Reactants used in FGD Systems and Potential Reactions

In FGD systems, the active part in natural limestone, which reacts with SO_2, is calcite ($CaCO_3$). Aside from calcite, limestone also contains Magnesite ($MgCO_3$), Silica (SiO_2), Alumina (Al_2O_3) and other impurities at low percentages [10]. When heated to a high temperature, calcite in limestone decomposes to quick lime (CaO) depending on the CO_2 partial pressure [10]:

$$CaCO_3(s) \rightarrow CaO(s) + CO_2(g) \qquad \Delta H^0 = 179.2\ kJ/mol \qquad \text{(R2.3)}$$

The calcination reaction (R2.3) occurs when calcite is heated to 700 ^{0}C and above. The reaction can be pushed to start at higher temperatures by raising the CO_2 partial pressure as shown in Figure 2.1. If the CO_2 partial pressure is increased from 0 kPa to 20 kPa, the calcination reaction begins to occur at 800 ^{0}C. At 50 kPa of CO_2, the minimum calcination temperature increases to 850 ^{0}C and at 100 kPa, it becomes 890 ^{0}C [10].

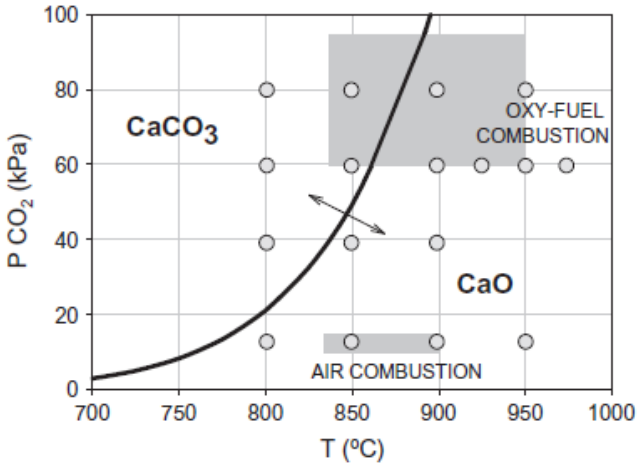

Figure 2.1: Thermodynamic equilibrium curve of $CaCO_3$ calcination with the dots referring to the experimental conditions of sulfation performed by [10].

Depending on whether the temperature and CO_2 partial pressure are favorable for calcination, sulfation in the FGD system would happen directly with calcite through:

$$CaCO_3(s) + SO_2(g) + 1/2O_2(g) \rightarrow CaSO_4(s) + CO_2(g) \qquad \Delta H^0 = -323.6\ kJ/mol \qquad \text{(R2.4)}$$

Or indirectly via calcination (R2.3) followed by lime sulfation:

$$CaO(s) + SO_2(g) + 1/2O_2(g) \rightarrow CaSO_4(s) \qquad \Delta H^0 = -502.8\ kJ/mol \qquad \text{(R2.5)}$$

In wet FGD, the hydrated lime ($Ca(OH)_2$) is produced by reaction of lime (CaO) with water.

$$CaO(s) + H_2O(g) \rightarrow Ca(OH)_2(s) \qquad \Delta H^0 = -108.5\ kJ/mol \qquad \text{(R2.6)}$$

The produced $Ca(OH)_2$ can then react with SO_2 as follows:

$$Ca(OH)_2(s) + SO_2(g) + 1/2O_2(g) \rightarrow CaSO_4(s) + H_2O(g) \qquad \Delta H^0 = -394.3\ kJ/mol \qquad \text{(R2.7)}$$

2.4.3 Experimental Studies of FGD Systems

In the literature (e.g. [11-15]), many researchers have studied the desulfurization of flue gas emitted from coal combustion. The studies were performed at a lab-scale where reactors were designed to study the effect of various conditions on the conversion of SO_2 to gypsum.

For example, Dam-Johanson et al. described research performed in three FGD reactors at different scales [11]. The purpose of their work was to evaluate the effectiveness of their reactors and to test the sulfation degree of a wide range of available natural limestone samples. The first reactor used was a laboratory-scale quartz reactor (~3 cm diameter - 63 cm height) mounted in an electrically heated oven with an external recirculation loop. The second reactor was a larger stainless-steel fluidized-bed reactor (~5 cm diameter) with an inert quartz sand bed. The third was a coal-fired fluidized bed pilot plant with thermal rating of 200 kW. It was fired with 25 kg/h of coal, which contains less than 1 % sulfur to mimic industrial operation. In all of the three reactors, limestone samples were added after the desired operating temperature of 850 ^{0}C was reached. The synthetic flue gas used in the two lab-scale reactors was a mixture of nitrogen, oxygen (~4 %), carbon dioxide (~10 %) and sulfur dioxide at less than 0.15 %. The only gas fed to the pilot plant was air to support the coal combustion; and the SO_2 emitted from coal was at ~0.04 %. The degree of sulfation obtained in the experiments was determined by measuring sulfur concentration in the flue gas, through a gas analyzer. Degree of sulfation was also determined from the change in mass of the limestone after the reactor runs. The results showed that there is an important influence of the physical texture of limestone on the degree of sulfation, such a way that limestone of a younger geological age acted better than older, compact and non-porous types. The best limestone showed a sulfation degree of a maximum of 80 %.

To study the kinetics of direct sulfation, Hu et al [12] built a quartz fixed-bed reactor with inner tube diameter of 1.6 cm, which was developed based on the one used by Dam-Johanson et al. [11]. The reactor consisted of a quartz shell with an inner removable quartz tube that contains the sample. The reactor was surrounded with an electrical heater. The mixture of N_2, O_2 (1.5-20 %) and CO_2 (8-45 %) entered the sample tube with SO_2 at 0.03-0.18 %. The gas mixture exited the reactor through a gas analyzer to measure its composition. The gas mixture flow was at 1 L/min through the bed containing 1 g of limestone, at temperatures varied between 500 and 600 ^{0}C (at which calcination does not yet occur). The absorption rate was studied in function of time in a 60 s duration. When increasing the SO_2 concentration from 0.03 to 0.18 % in the gas mixture, the absorption rate increased three times, especially in the first 20 s. Increasing the O_2 concentration from 1.5 to 20 %, resulted in doubling the conversion rate [12].

Siagi et al. built a stainless-steel fixed-bed reactor, where 0.1 g of the sorbent was dispersed in 3 g of silica sand to achieve larger surface area of contact between the gas and the sorbent [13]. The silica-sorbent mixture rested on glass wool in the middle of the tube, which was fitted in the middle of a furnace. The temperature varied between 60 and 80 ^{0}C. The sorbent used was $Ca(OH)_2$ prepared from limestone, which was first calcined to lime (CaO) at 900 ^{0}C for 3 h, before being hydrated to $Ca(OH)_2$. The gas mixture, introduced from the top of reactor, consisted of N_2, O_2, SO and SO_2, where N_2 was first passed through a humidifier. Using a gas analyzer, Siagi et al. recorded the duration of retention of SO_2 by the sorbent $Ca(OH)_2$ to study the sorption capacity of different types of "treated" limestone. For a gas flow of 150 ml/min containing 0.2 % SO_2, the retention duration varied between 2 and 12 minutes depending on the type of limestone from which hydrated lime was formed [13]. The results of sulfation showed that in temperatures of 60 to 80 ^{0}C, the maximum absorption was of 18 % for some types of limestone and was as low

as 2 % for limestone of poor calcite content; By comparison, commercial hydrated lime made of pure $Ca(OH)_2$ resulted in 10 % absorption at these low temperatures.

2.4.4 Quantitative Analysis of Product from FGD Systems

A common method to analyze qualitatively the chemical composition of the sorbent sample is X-ray Diffraction (XRD) analysis, which was used by Siagi et al. [13] as well as by Bigham et al. [14] and Chen et al. [15]. XRD is generally used for qualitative analysis, but has been used to obtain approximate quantitative compositions of samples tested, given enough information about the surface area and structure of the compounds. For example, Siagi et al. used a semi-quantitative XRD technique to test for portlandite ($Ca(OH)_2$), hannebachite ($CaSO_3.0.5H_2O$) and magnesium sulfite hydrate ($MgSO_3.6H_2O$), major products found from reaction of hydrated lime with SO_2. Bigham et al. tested for the products of various FGD processes [14]. A larger variety of minerals was found, including anhydrite ($CaSO_4$), gypsum ($CaSO_4.2H_2O$), portlandite ($Ca(OH)_2$), lime (CaO) and hematite (Fe_2O_3). The highest amounts of anhydrite were found in the products from fluidized bed combustor followed by dry lime injection multistage burner (LIMB). Duct injection and spray dryers, which are wet FGD systems, have showed production of hannebachite, showing that wet FGD systems requires extra oxidation step to produce saleable gypsum ($CaSO_4.2H_2O$).

In addition to XRD analysis, thermogravimetric analysis (TGA) has also been used by researchers for testing experimental samples of solid products from FGD systems. Bigham et al. showed a "thermogram" representation of the weight loss that occurred over time when solid product samples were heated using a heating rate of 20 ^{0}C/min, under nitrogen atmosphere [14]. The mass losses occurring at various temperature ranges were associated with the decomposition and gasification of various components in the sample. A weight loss in the temperature range of 300

to 370 ^{0}C, is associated with the evolution of water from hannebachite ($CaSO_3.0.5H_2O$). Portlandite ($Ca(OH)_2$) conversion to lime (CaO) occurs in a temperature range of 375 to 500 ^{0}C. Calcite ($CaCO_3$) and dolomite ($CaMg(CO_3)_2$) thermally decompose in the temperature range of 600 to 850 ^{0}C resulting in CO_2 evolution. Anhydrite ($CaSO_4$), lime (CaO) and magnesia (MgO) are thermally stable and do not decompose over the range of temperatures utilized during the TGA runs; however, Bigham et al. observed mass loss of their anhydrite sample, in the range of 850-1050 ^{0}C and related it to the anhydrite reaction with elemental char carbon that was present in the sample [14].

2.4.5 Results from Desulfurization Experiments in Literature and Effect of Various Conditions

As seen, XRD and TGA analyses are two key methods used for studying the sulfation degree and the effect of key operating conditions on conversion. For instance, the effect of temperature is studied by Garcia-Labiano et al. by flowing SO_2 on a calcite sample in a TGA apparatus [10]. The SO_2 flowing into the pan was at 0.3 % in a CO_2/O_2 gas mixture containing 60 % CO_2. The results showed that after 18 hours, the sulfation degree was 0.5 at 850 ^{0}C, higher than 0.4 at 800 ^{0}C. At these two temperatures with a CO_2 partial pressure of 60 kPA, direct sulfation occurred via R2.4 (i.e., no calcination) and the effect of increasing the temperature resulted in an increase of conversion. At an increased temperature of 900 ^{0}C, sulfation degree increased further to 0.7. At temperatures at 900 ^{0}C and up to 975 °C, indirect sulfation occurs and degree of sulfation was almost independent of the change in temperature up to 5 h; with longer hours, the effect of temperature was more shown and the degree of sulfation was slightly smaller for higher temperatures than at 900 °C. The higher conversion at temperatures of 900 ^{0}C and above was due to the calcination of $CaCO_3$ to CaO, which has higher porosity and allows better access of gas

into the particle. However, increasing temperature to above 900 ^{0}C results in sintering effect, and therefore, increased heat exposure at high temperatures decreased again the conversion in function of temperature [10]. In conclusion, the optimal temperature for sulfation was at 900 ^{0}C, for the specific CO_2 concentration of 60 % at atmospheric pressure. [10].

Furtes et al. in their work studied the influence of temperature between 750 ^{0}C and 900 ^{0}C on the sulfation reaction, with a CO_2 concentration of 96 % and a SO_2 concentration of 0.25 % (oxygen balanced) [16]. Similar to results of Chen et al. [15], sulfation degree increased from 0.3 to 0.8 as a function of temperature, showing a significant increase between 850 ^{0}C and 900 ^{0}C. This behavior is due to the change from uncalcined to calcined state resulting in change from direct to indirect sulfation. The effect of temperature on conversion was shown to be similar for the various particle sizes.

To show whether changing the CO_2 concentration had an effect on the optimal temperature for sulfation, Garcia-Labiano et al. conducted tests at various CO_2 concentrations for temperatures of 800, 850 and 900 ^{0}C [10]. It was shown that when varying CO_2 concentration in a range that allowed only direct calcination at a given temperature (e.g. 800 ^{0}C), the effect of changing the CO_2 concentration was unnoticeable and the conversion percentage stayed equal to 0.4. Similarly, at a higher temperature (e.g. 900 ^{0}C), when changing the CO_2 concentration in a range that always allows calcination and therefore indirect sulfation, the conversion was also constant but at a higher value of 0.8 that did not vary with the change in the CO_2 concentration. Further experience, where the CO_2 concentration changed the calcination conditions from calcined to uncalcined at the temperature of 850 °C, showed a decrease in the conversion from 0.8 to 0.4 due to the transfer from indirect to direct sulfation [10]. In conclusion, Garcia-Labiano's tests showed that CO_2 concentrations have effects on the sulfation degree through its effect on the calcination

conditions; if concentration of CO_2 was higher than the equilibrium concentration for a given temperature (as shown in Figure 2.1), calcination to CaO would not occur and direct sulfation of $CaCO_3$ would result in lower degree of sulfation.

Illerup et al. studied the effects of total pressure and CO_2 partial pressure on the sulfation reaction [17]. At 750 ^{0}C, sulfation was not affected noticeably by the pressure change and was stable around 0.7, as the total pressure was varied such a way that $CaCO_3$ was uncalcined for all pressures.

At 850 ^{0}C, a drop in the degree of sulfation from 0.8 to 0.3 was observed when CO_2 partial pressure and total pressure increased, indicating that a change from calcined to uncalcined limestone occurred. The explanation for the curve of sulfation at 850 ^{0}C was as follows: at atmospheric temperature, $CaCO_3$ is calcined to CaO and resulted therefore in a sulfation degree of 0.8, higher than that at 750 ^{0}C that averaged 0.7. When pressure of CO_2 was increased above 60 kPa, $CaCO_3$ was not able to calcine to CaO; $CaCO_3$ is affected more by sintering than CaO at this temperature, and therefore sulfation dropped in value to 0.3.

At 950 ^{0}C, an increase in the total pressure resulted in an increase in the degree of sulfation; at this temperature and for all the pressures, $CaCO_3$ is calcined to CaO regardless the pressure of CO_2 and therefore resulted in a conversion curve different than that at 850 ^{0}C: at atmospheric pressure, the sulfation was 0.5 due to the sintering effect at 950 °C. Increasing the total pressure to 10 bars increased the sulfation at this temperature from 0.5 to 0.8; the only explanation to the increase of sulfation at this temperature was the increase of SO_2 pressure with the total pressure resulting therefore in a higher sulfation degree.

In conclusion, this study shows the opposing effects of sintering and calcination that happen both with the increase in temperature; these two factors should be well taken into consideration when deciding on the process conditions, especially when CO_2 concentration is increased [17].

A more noticeable effect that Illerup et al. also showed was that of heat treatment of limestone before sulfation. For example, when calcite was heated for 15 min at 850 ^{0}C, its sulfation degree dropped to half compared to when no heat treatment was used. Illerup et al. explained the change in the sulfation degree by the sintering effect of prolonged heating [17].

Wang et al. studied the influence of the water content in the flue gas on limestone sulfation [18]. Calcined limestone can react with water vapor to produce $Ca(OH)_2$ through R2.6. At high temperatures such as 800 and 850 ^{0}C, R2.6 is not a thermodynamically stable reaction; however, Wang et al. suggested that in presence of water vapor, $Ca(OH)_2$ is formed as an intermediate and is able to react with SO_2 via R2.7. The results of sulfation were compared for water conditions of 0 and 0.1. Known for its reactive nature, $Ca(OH)_2$ was able to increase the sulfation degree by 0.05 when it was formed intermediately in presence of water vapor [18].

The effects of particle size were studied by Garcia-Labiano et al. [10], Furtes et al [16] and Wang et al. [18]. Furtes et al. showed that smaller particles (e.g., ~150 μm) result in a higher sulfation degree (0.6 at 850 ^{0}C after 180 min) compared to larger particles (e.g., ~425 μm) that resulted in sulfation degree of only 0.3 at the same temperature. Wang et al. showed that particle size of 75-150 μm had a higher degree of sulfation averaging 0.3, compared to the lower value of 0.17 for bigger particle size of 250-425 μm.

Finally, the direct effect of increasing SO_2 concentration was studied by Garcia-Labiano [10]. As expected, an increase in SO_2 concentration in both calcined and uncalcined conditions resulted in

an increase in sulfation degree. In calcined conditions, sulfation increased from 0.2 to 0.8 when SO_2 concentration increased from 500 to 5000 ppm after 20 h with a flow of 10 L/h. In uncalcined conditions, sulfation degree increased from 0.1 to 0.5 when SO_2 concentration increased from 1000 to 5000 ppm. This behavior was also noted by Illerup et al., who increased the total pressure in their experiments, and thereby increased the SO_2 partial pressure, while maintaining the same CO_2 partial pressure; the conversion increased from 0.4 to 0.7 when partial pressure of SO_2 increased ten times, at 850 ^{0}C, in calcined conditions [17].

In summary, FGD systems for removal of SO_2 from flue gas have been well studied in the literature and the effects of different operating parameters have been explained using results from a variety of laboratory experiments. The tests have shown that using dry FGD is better than wet FGD as it allows the formation of fully oxidized $CaSO_4.2H_2O$ rather than $CaSO_3.0.5H_2O$. When the used sorbent is limestone, higher temperature results in higher degree of sulfation up to 0.9 as limestone calcines first to CaO. At low CO_2 partial pressure under calcination conditions, the optimum temperature for sulfation is 850 ^{0}C; however, increasing the CO_2 pressure to above the calcination equilibrium line results in direct sulfation of $CaCO_3$ that results in a lower degree of sulfation. The reason for the better performance of CaO compared to $CaCO_3$ is that CaO is more porous, and is less sintered at high temperatures. Above 900 ^{0}C, CO_2 concentration does not affect calcination that occurs at all concentrations. Higher temperatures than 900 ^{0}C risk a higher sintering effect on CaO and therefore can result in a lower sulfation degree.

2.5 References for Chapter 2

[1] Rappold TA, K.S. Lackner KS, Large scale disposal of waste sulfur: From sulfide fuels to sulfate sequestration, Energy. 35 (2010) 1368-1380.

[2] Galloway JN. Anthropogenic mobilization of sulfur and nitrogen: immediate and delayed consequences. Annual review of energy and the environment. 21 (1996) 261-292.

[3] Stern DI, Reversal of the trend in global anthropogenic sulfur emissions, Global Environ. Change. 16 (2006) 207-220.

[4] Song C. An overview of new approaches to deep desulfurization for ultra-clean gasoline, diesel fuel and jet fuel. Catalysis Today 86 (2003) 211-263.

[5] Natural Resources Canada. Environmental impacts of combustion. (2013). Retrieved from: http://www.nrcan.gc.ca/energy/publications/efficiency/industrial/cipec/6695

[6] Abedini R, Salooki MK et al. Modeling and simulation of condensed sulfur catalytic beds of claus process: rapid estimation. Chemical Engineering Research Bulletin 14 (2010) 110-114.

[7] Srivastava RK. Flue gas desulfurization; the state of the art. Air and waste manage. 51 (2001) 1676-1688.

[8] Katolicky J, Jicha M. Influence of the lime slurry droplet spectrum on the efficiency of semi-dry flue gas desulfurization. Chem. Eng. Technol. 36-1 (2013) 156-166.

[9] Kost DA, Bigham JM, Stehouwer RC et al. Chemical and physical properties of dry flue gas desulfurization products. Jounal of environmental quality. 34 (2005) 676-686.

[10] Garcia-Labiano F, Rufas A, deDiego LF et al. Calcium-based sorbents behaviour during sulphation at oxy-fuel fluidised bed combustion conditions. Fuel 90 (2011) 3100-3108.

[11] Dam-Johansen K, Ostergaard K. High temperature reaction between sulphur dioxide and limestone-I.Comparison of limestones in two laboratory reactors and a pilot plant. Chemical Engineering Science 46-3 (1991) 827-837.

[12] Hu G, Dam-Johansen K, Wedel S. Kinetics of the direct sulfation of limestone at the initial stage of crystal growth of the solid product. AIChE 57-6 (2011) 1607-1616.

[13] Siagi ZO, Mbarawa M, Mohamed AR et al. The effects of limestone type on the sulphur capture of slaked lime. Fuel 86 (2007) 2660-2666.

[14] Bigham JM, Kost DA, Stehouwer RC et al. Mineralogical and engineering characteristics of dry flue gas desulfurization products. Fuel 84 (2005) 1839-1848.

[15] Chen J, Yao H, Zhang L. A study on the calcination and sulphation behaviour of limestone during oxy-fuel combustion. Fuel 102 (2012) 386-395.

[16] Furtes AB, Velasco G, Fuente E et al. Study of the direct sulfation of limestone particles at high CO2 partial pressures. Fuel Processing Technology 38 (1994) 181-192.

[17] Illerup JB, Dam-Johansen K, Lunden K. High temperature reaction between sulphur dioxide and limr-VI The influence of high pressure.

[18] Wang C, Jia L, Tan Y et al. The effect of water on the sulphation of limestone. Fuel 89 (2010) 2628-2632.

Chapter 3

Sulfur as a Fuel Source in a Combined Power Cycle Equipped with Dry Flue Gas Desulfurization System

3.1 Background

Through the last decades, sulfur has been largely produced as a by-product from petroleum refineries resulting in a drastic reduction in sulfur mining [1]. The reason behind this extensive production is the environmental concerns regarding sulfur emissions into the atmosphere from fuel combustion and the resultant acid rain. Fort McMurray Alberta is an example of this type of sulfur production where more than 9 Mt of sulfur are stored in elemental solid form [2]. To reach this state, sulfuric compounds in the fuel undergo a first step of hydrogenation to hydrogen sulfide (H_2S), followed by Claus process to convert H_2S to an elemental sulfur (S) [3,4]. This type of storage is by definition temporary as sulfur in elemental form is far from its thermodynamic ground-state and will eventually form other compounds.

Unlike petroleum refineries, where sulfur is removed in a pre-combustion process, coal power plants combust sulfur then mitigate SO_2 emissions in a post-combustion process called Flue Gas Desulfurization (FGD) [5]. To prevent its emission into the atmosphere, the FGD system scrubs the flue gas with limestone, which is composed of calcite ($CaCO_3$) that reacts with SO_2:

$$CaCO_3(s) + SO_2(g) + 1/2O_2(g) \rightarrow CaSO_4(s) + CO_2(g) \qquad \Delta H^0 = -324.2\ kJ/mol \qquad \text{(R3.1)}$$

The use of limestone as a sorbent instead of hydrated lime ($Ca(OH)_2$) has been of industrial interest due to the limestone's lower cost and its availability as a raw material; the type of FGD used for this reaction is dry FGD where limestone is burned with SO_2 in a boiler. More information about various types of FGD and their applications is available in the literature [6-13]. The dry FGD reaction produces anhydrite ($CaSO_4$) that, if hydrated, is called "synthetic" gypsum to differentiate it from natural mined gypsum [14]. Gypsum is used in the production of Portland cement, plasters and wall-board. It is as well a soil conditioner for agriculture fertilization [15].

In this study, elemental sulfur is converted to anhydrite in a two-stage process; the first is based on the sulfur oxidation reaction shown as follows:

$$S(s) + O_2(g) \rightarrow SO_2(g) \quad \Delta H^0 = -296.8\ kJ/mol \tag{R3.2}$$

In the second stage, SO_2 is reacted with $CaCO_3$ available from natural limestone, to produce anhydrite in a dry FGD system as per (R3.1); the overall reaction would then be:

$$CaCO_3(s) + S(s) + 3/2\ O_2(g) \rightarrow CaSO_4(s) + CO_2(g) \quad \Delta H^0 = -620.4\ kJ/mol \tag{R3.3}$$

The two sub-reactions (R3.1) and (R3.2) are exothermic, suggesting that energy recovery is feasible and a thermodynamic study is necessary to evaluate the amount of electrical energy that can be recovered from the sum of the two reactions. The summation of these two reactions can present an alternative for elemental sulfur stockpiling that is becoming an environmental burden [16]. The objective of this work is not to only convert sulfur to the stable form anhydrite, but to also produce electrical power. Sulfuric acid plants already produce electrical power from the energy emitted in the conversion of H_2S to H_2SO_4 providing 793 kJ/mol of heat [17].

This analysis considers electricity production from a gas turbine combined cycle that will be referred to as a Sulfur Combined Cycle (SCC). The fact that sulfur combustion produces the

gaseous SO_2 with no other solid products was a reason to study electrical power production in a gas turbine. The SCC will be based on the technology of Natural Gas Combined Cycle (NGCC), in which the fuel used is natural gas (NG) instead of sulfur. NGCC is used as a basis for the analysis as it is currently the state-of-the-art in large-scale electricity production [18]. In typical NGCC plants, the turbine is equipped with a heat recovery steam generator (HRSG) of a three-pressure level with reheat type (See Figure 3.1). The HRSG helps by increasing the total efficiency of the system, here defined as total electrical work produced over total available thermal energy [19].

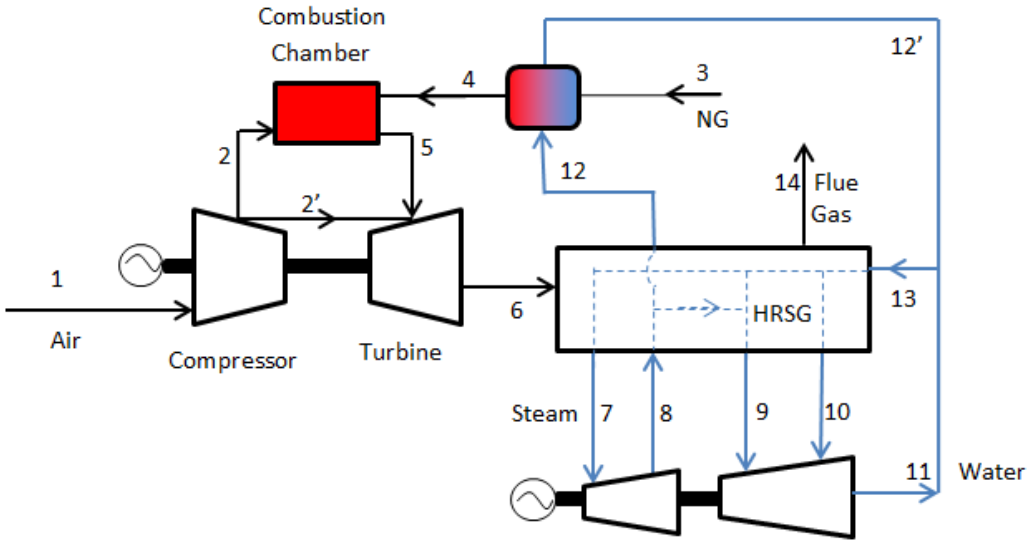

Figure 3.1: Natural gas combined cycle (reference case). Black line is the gas stream and blue line is the water stream.

The Reference Case is compared with three different SCC Cases (Case 1, Case 2a and Case 2b). In the three options, sulfur is oxidized to SO_2 using compressed dry air (R3.2). Similarly to the

Reference Case, HRSG system is added for extra heat recovery from the flue gas. In a SCC, a FGD system is required to prevent SO_2 emissions to the atmosphere. The FGD system can be added before or after the HRSG unit. In the first studied case (Case 1), the FGD system was at the end of the process, downstream of the HRSG; in Cases 2a and 2b, the FGD system was moved upstream of the HRSG to analyze the capability of recovering additional heat from the flue gas leaving the FGD, and entering the HRSG. The difference in Case 2b from Case 2a is that the turbine outlet temperature (TOT) was lowered to increase energy recovery from the gas turbine. Thermodynamic calculations based on this process configuration can be used to make recommendation for ongoing research into energy recovery and anhydrite production from sulfur.

3.2 Process Analysis

3.2.1 Natural Gas Combined Cycle Plant (Reference Case)

The NGCC Reference Case modeled in this study is based on the version considered by Manzolini et al. [20]. Their base case-study plant involves two natural gas turbines based on a Brayton cycle and a single HRSG turbine of a Rankine cycle, which result in 829.9 MW of electrical generation. The Reference Case in this study considered a single NG turbine and one HRSG, reducing the expected power output into half. The Reference Case NGCC plant is also similar to a single-gas-turbine combined cycle used by Amrollahi et al. [21].

Assumptions related to the case study simulations are shown in Table 3.1 and the thermodynamic equations used are provided in Table 3.2. Stream mass flow rates, temperatures, pressures and compositions for this Reference Case are presented in Table 3.3. As shown in Figure 3.1, air from Stream 1 is pressurized in the compressor before entering the combustion chamber, at a temperature of 417 ^{0}C. Natural gas in Stream 4 enters the combustion chamber after preheating to

160 ^{0}C by a heat exchanger [20]. In the adiabatic combustion chamber, the exothermic combustion reaction of NG increases the temperature to a combustor outlet temperature (COT) of 1443 ^{0}C. A fraction (19.5%) of the compressed air bypasses the combustion chamber via Stream 2' to cool the turbine, lowering the value of the turbine inlet temperature (TIT) to a temperature of 1270 ^{0}C. The gas mixture expands in the turbine and produces work that is converted to electricity.

To increase the efficiency of the cycle, Stream 6 is fed to a three-pressure level HRSG where the flue gas heats a water stream in a counter-current fashion. All of the liquid water that enters the HRSG (Stream 13) is pumped and evaporated to produce low pressure (LP) steam at 3.5 bar and 299 ^{0}C. Then, 10 % of this steam is fed to the LP turbine via Stream 10. The stream containing 70 % of the inlet water is pressurized to a high pressure (HP) of 121 bar. It absorbs a large fraction of the heat from the flue gas, producing Stream 7 at 560 ^{0}C. Stream 8 exits the HP turbine at 338 ^{0}C and a lower pressure of 28 bar. Stream 8 is reheated in the HRSG and 91 % of it is combined with the intermediate pressure (IP) stream (containing 20 % of the inlet water) to form Stream 9 at 561 ^{0}C and 23 bar. Stream 9 enters the IP turbine and produces work as it expands to give Stream 11 which exits the turbine at 32 ^{0}C. Stream 14 is the 9 % of Stream 8 used to preheat natural gas to 160 ^{o}C.

Solving the equations in Table 3.2 gives a predicted total power output of 410 MW. This power production is slightly less than half of Manzolini's value (830 MW) [20], and higher than the value reported by Amrollahi et al. (384.4 MW) for a similar size single-gas turbine plant [21]. The overall thermal efficiency of 58.1 %, based on the lower heating value (LHV) calculated for the plant in Figure 3.1, is similar to the value reported by Manzolini et al. (58.3 %) and higher than 56.4 % (LHV), the value of Amrollahi et al. These results suggest that the NGCC plant

model is a reasonable basis for calculations involving the SCC plants models described in Case 1, Case 2a and Case 2b.

Table 3.1: Main assumptions used for modelling the processes.

#	**Assumptions**
1	*Air*: Dry molar fraction [%] O_2 20.95, N_2 78.08, CO_2 0.04, Ar 0.93. For the Reference Case, the air has a relative humidity of 60 %. For case 1 and cases 2a and 2b, the air is assumed to be dry.
2	*Natural Gas*: molar fraction [%] CH_4 89.0, C_2H_6 7.0, C_3H_8 1.0, C_4H_{10} 0.1, N_2 0.9, CO_2 2.0. The standard enthalpy of combustion for the NG is 837.6 kJ/mol (LHV).
3	*Sulfur:* Specific heats of liquid and solid sulfur are provided from Table IX in [22]. ΔH of fusion is equal to 1.61 kJ/mol, at melting point of 119.6 ^{0}C.
4	*Turbine and compressors:* the work done by the turbine is positive. 19.4 % of the air exiting the compressor is used to cool the inlet to the gas turbine.
5	*Combustion and energy:* Adiabatic combustion is assumed in combustion chamber and FGD. Kinetic and potential energy changes are negligible in the evaluation of energy flow. Ideal-heat capacities are used in the evaluation of enthalpies where effect of pressure is neglected. Enthalpies of formation for species are used from [26]. Constants in the evaluation of specific heat are used from [27]. Complete combustion is assumed in the combustion chamber and the FGD unit.
6	*HRSG/steam turbines*: Efficiency of heat transfer from flue gas to water in the HRSG is 35.6 % found from [20] in Reference Case and is used in tuning Cases 1 and 2 to find steam turbines water work where the temperature of water/steam in the different streams is matching with the Reference Case by changing the mass flow. Mass fraction of steam entering HP, IP and LP turbines are 70, 84 and 10 % respectively. Enthalpy values for water/steam were obtained from steam table in [26].

Table 3.2: Equations used for modelling the NGCC and SCC processes.

#	Equation name	Equation
1	Enthalpy of gas mixture in k^{th} stream	$\Delta\dot{H}_k = \sum_i \Delta\dot{H}_i(T_k) = \sum_i \dot{n}_i \int_{298.15}^{T_k} C_{p,i}^{ig} dT$ $where\ \frac{C_{p,i}^{ig}}{R} = A_i + B_i T + C_i T^2 + D_i T^{-2}$
2	Standard enthalpy change due to combustion (LHV)	$\Delta\dot{H}^0{}_{comb,\ unit} = \sum_i \dot{n}_{i,\ unit}\left(v_i \Delta H^0{}_{fi}\right)$
3	Total standard enthalpy released by reactions	$-\Delta\dot{H}^0{}_T = -\sum_{unit=CC,\ FGD} \Delta\dot{H}^0{}_{comb,\ unit}$
4	Enthalpy change between inlet and outlet streams for a unit	$\Delta\dot{H}_{unit} = \sum_{k\ out} \Delta\dot{H}_{k\ out} - \sum_{k\ in} \Delta\dot{H}_{k\ in}$
5	Energy balance on combustion chamber and FGD	$\Delta\dot{H}_{unit} + \Delta\dot{H}^0{}_{comb,\ unit} = 0$
6	Power of compressor	$\dot{W}_{comp} = -\Delta\dot{H}_{comp}$
7	Power of turbine	$\dot{W}_{turb} = -\Delta\dot{H}_{turb}$
8	Power of steam turbines	$\dot{W}_{steam} = -\sum_{unit=HP,IP,LP} \Delta\dot{H}_{unit}$
9	Net work from the compressor and turbine	$\dot{W}_{net} = \dot{W}_{turb} + \dot{W}_{comp}$
10	Total work by combined cycle	$\dot{W}_T = \dot{W}_{turb} + \dot{W}_{comp} + \dot{W}_{steam}$
11	Electrical Efficiency	$\eta_{th} = \frac{\dot{W}_T}{-\Delta\dot{H}^0{}_T}$
12	Fraction of enthalpy from flue gas converted to work in HRSG	$\eta_{HRSG} = \frac{\dot{m}_{water}\left[x_{HP}(H_8 - H_7) + x_{IP}(H_{11} - H_9) + x_{LP}(H_{11} - H_{10})\right]}{(\Delta\dot{H}_{14} - \Delta\dot{H}_6)}$
13	Sulfur Enthalpy in Stream 4	$\Delta\dot{H}_4 = \dot{n}_S \int_{T_{25\,^0C}}^{T_{119.6\,^0C}} C_{p,\ S(s)} dT + \dot{n}_S h_{m,S}(119.6\,^0C) + \dot{n}_S \int_{T_{119.6\,^0C}}^{T_{160\,^0C}} C_{p,\ S(l)} dT$

Table 3.3: Mass flow rate, pressure, temperature and composition of main streams in NG reference case adapted from [20].

Stream	$\dot{m}$	**T**	**P**	**Composition (% mol)**				
	(kg/s)	**(^{0}C)**	**(bar)**	**Ar**	**N_2**	**O_2**	**CO_2**	**H_2O**
1	650	15	1	0.92	77.31	20.74	0.04	0
2	523	417.5	18.16	0.92	77.31	20.74	0.04	0
3	15.3	10	70	See NG composition in Table 1				
4	15.3	160	70					
5	539	1443 (COT)	17.6	0.88	73.72	11.06	4.88	10.04
6	665	608	1.04	0.89	73.72	10.48	3.97	8.34
7	76.9	559.5	120.9	-	-	-	-	100
8	76.9	337.7	28	-	-	-	-	100
9	92.5	561.0	22.96	-	-	-	-	100
10	21.9	299	3.52	-	-	-	-	100
11	109	32.2	0.048	-	-	-	-	100
12	6.58	230	28	-	-	-	-	100
13	110	32.2	1	-	-	-	-	100
14	665	86.8	1.01	0.89	74.40	12.40	3.97	8.34

Total Power Output ($\dot{W}$)	**Net Electricity Efficiency (η)**	**CO_2 emission**
410 MW	58.1 %	0.36 kg CO_2/kWh

3.2.2 Sulfur Combined Cycle with no FGD Heat Recovery (Case 1)

Consider the SCC system shown in Figure 3.2 (Case 1), where the inlet air used has the same mass flow as in the Reference Case (See Table 3.4). Case 1 differs from the Reference Case in that sulfur is the fuel used rather than natural gas, and that a FGD system is added to desulfurize the flue gas after it exists the HRSG. Sulfur is first heated to 160 ^{0}C similarly to NG, and then injected into the combustion chamber as a liquid. The enthalpy of sulfur in Stream 4 can be calculated from Eqn. 13 in Table 3.2.

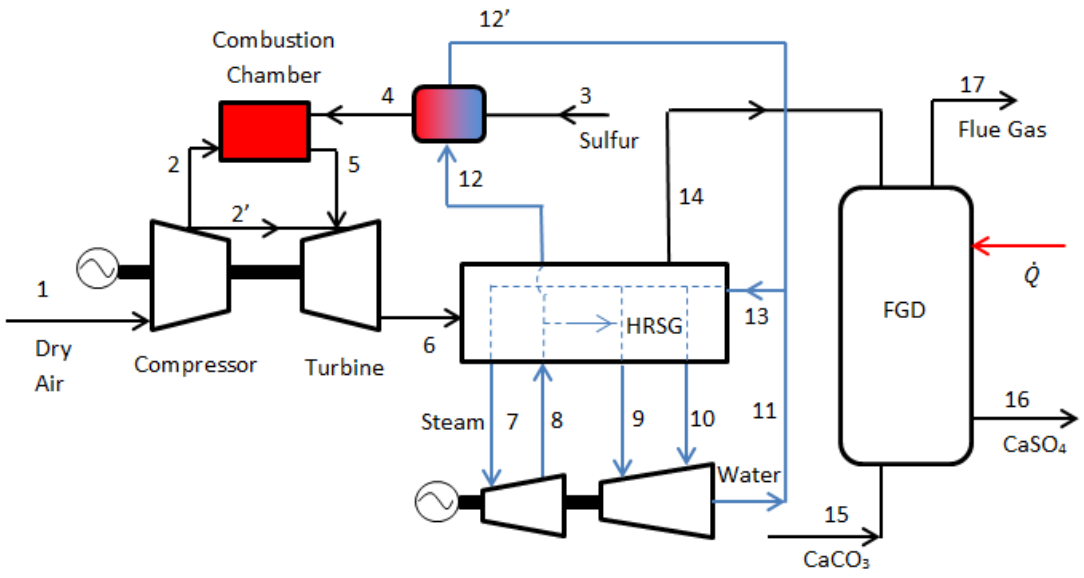

Figure 3.2: Sulfur combined cycle with no heat recovery from FGD in HRSG (Case 1). Black line is the gas stream and blue line is the water stream. Red line is the heat stream.

To match a combustor outlet temperature (COT) of 1443 ^{0}C as in the Reference Case, the mass flow of sulfur required for combustion was 72 kg/s, ~5 times greater than that of NG required to heat the same 650 kg/s of compressed air.

The gas mixture expands in the turbine and drops in temperature to a turbine outlet temperature (TOT) of 608 ^{o}C in Stream 6 that matches the Reference Case. The gas turbine produces 253 MW of net work (see Eqn. 9 in Table 3.2), a value slightly smaller than that in the Reference Case owing to the difference in the flue gas composition between NGCC and SCC.

Table 3.4: Mass flow rates, pressure, temperature and composition of main streams of sulfur combined cycle with no heat recovery from FGD in HRSG (Case 1).

Stream	$\dot{m}$	**T**	**P**	**Composition (%mol)**					
	(kg/s)	**(^{0}C)**	**(bar)**	**Ar**	**N_2**	**O_2**	**CO_2**	**H_2O**	**SO_2**
1	650	15	1	0.93	78.08	20.95	0.04	0	0
2	523	417.5	18.16						
3	72.0	25	1.01	Elemental Sulfur (100 %)					
4	72.0	160	1						
5	596	1328 (COT)	17.6	0.93	78.08	8.41	0.04	0	12.54
6	722	608	1.04	0.93	78.08	10.92	0.04	0	10.03
7	75.1	559.5	120.9	-	-	-	-	100	-
8	75.1	337.7	28	-	-	-	-	100	-
9	90.1	561	22.96	-	-	-	-	100	-
10	10.7	299	3.52	-	-	-	-	100	-
11	101	32.2	0.048	-	-	-	-	100	-
12	6.4	230	28	-	-	-	-	100	-
13	107	32.2	1	-	-	-	-	100	13
14	722	87	1.01	0.93	78.08	10.92	0.04	0	10.03
15	225	25	1	Calcium Carbonate (100 %)					
16	306	900	1	Calcium Sulfate (100 %)					
17	641	900	1	0.98	82.20	6.22	10.60	0	0

Total Power Output ($\dot{W}$)	**Net Electricity Efficiency (η)**	**CO_2 emission**
342 MW	24.5 %	1.045 kg CO_2/kWh

The electrical efficiency of the HRSG from the Reference Case (η_{HRSG}= 35.6 %, see equation 12 in Table 3.2) was used to calculate the flow rate of feed water $\dot{m}_w$ required to match temperatures, pressures and flow-rate fractions (x_{HP}, x_{IP} and x_{LP}) within the HRSG. The thermal power going to the HRSG was 379 MW_{th}. As a result, the steam turbines produced an electrical power $\dot{W}_{HRSG}$ equal to 135 MW, similar to the Reference Case value of 138 MW.

The HRSG output gas mixture, at a temperature of 87 ^{0}C set to the Reference Case value, enters the FGD in Stream 14. A feed of calcite is added in Stream 15 to react with SO_2 through (R3.1) producing $CaSO_4$(s) in Stream 16. The optimal temperature for this reaction is 900 ^{0}C as shown by Garcia-Labiano et al. [23]. To reach that temperature in the FGD, an additional 126 MW_{th} is required beyond the heat released from (R3.1). This heat, shown as $\dot{Q}$ in Figure 3.2, can be supplied from the hot flue gas going to the HRSG, but would lower the thermal energy of the HRSG to 253 MW_{th}; and therefore, the electrical power of HRSG is dropped to 90 MW and the total (electrical) power output to 342 MW. As a result, the total electrical efficiency is 24.5 %. Note that in this case, there is no heat recovery from the FGD. The CO_2 emitted from this process is 1.05 kg/kWh, a value higher than the reference value of a new pulverized coal (PC) plant (0.762 kg/kWh) [24].

3.2.3 Sulfur Combined Cycle with FGD Heat Recovery

3.2.3.1 Turbine Outlet Temperature Matched to Reference Case (Case 2a)

To increase the heat recovery and reduce the CO_2 emissions per unit of energy, the FGD could be located upstream of the HRSG, as shown in Figure 3.3. The flue gas coming out of the gas turbine in Stream 6 is at 608 ^{0}C; therefore, if the flue gas is fed directly to the FGD, less energy

will be required to heat the mixture to the reaction temperature of 900 ^{0}C. This proposed change makes the process more efficient in that all of the thermal energy needed is provided by the desulfurization reaction (R3.1).

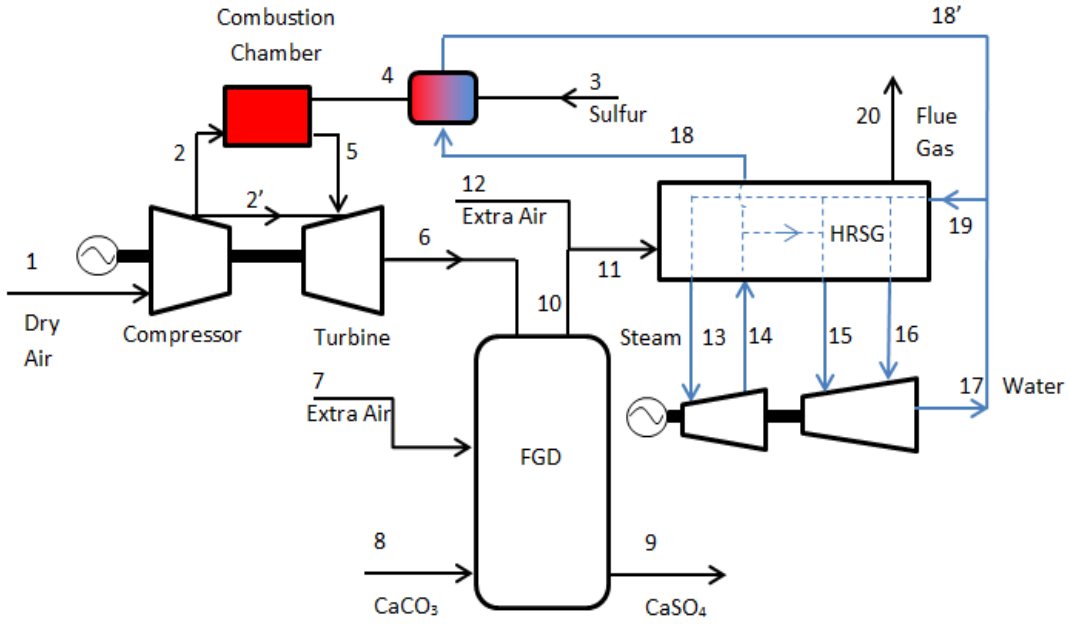

Figure 3.3: Sulfur combined cycle with Heat Recovery from FGD in HRSG (Cases 2a and 2b). Black line is the gas stream and blue line is the water stream.

Energy balance calculations show that the hot gas in Stream 6, when reacted with calcite from Stream 8, results in FGD temperature higher than the optimal value of 900 ^{0}C. To maintain the temperature at 900 ^{0}C, excess ambient air is added in Stream 7. The flue gas in Stream 10, which exits the FGD, is also mixed with ambient air to lower the gas temperature entering the HRSG and match the Reference Case value (608 ^{0}C).

The resulting mass flow rate of the flue gas in Stream 11 is higher than in the Reference Case, resulting in an increase of the mass flow of water required in HRSG to match temperature conditions of Reference Case. As shown in Table 3.5, the power output of the HRSG increases to

201 MW and the total power output is then 454 MW. The resulting CO_2 emissions decrease to 0.791 kg/kWh.

Table 3.5: Mass flow rates, pressure, temperature and composition of main streams of sulfur combined cycle with heat recovery from FGD in HRSG (Case 2a).

Stream	$\dot{m}$	**T**	**P**	**Composition (% mol)**					
	(kg/s)	**(^{0}C)**	**(bar)**	**Ar**	**N_2**	**O_2**	**CO_2**	**H_2O**	**SO_2**
1	650	15	1	0.93	78.08	20.95	0.04	0	0
2	523	516	18.16	0.93	78.08	20.95	0.04	0	0
3	72.0	25	1.01	Elemental Sulfur (100 %)					
4	72.0	160	1						
5	59	1328 (COT)	17.6	0.93	78.08	8.41	0.04	0	12.54
6	722	608	1.1	0.93	78.08	10.92	0.04	0	10.03
7	265	15	1	0.93	78.08	20.95	0.04	0	0
8	225	15	1	Calcium Carbonate $CaCO_3$ (100 %)					
9	306	900	1	Calcium Sulfate $CaSO_4$ (100 %)					
10	905	900	1.06	0.96	80.96	10.64	7.43	0	0
11	1015	608	1.04	0.96	80.64	11.79	6.61	0	0
12	110	15	1	0.93	78.08	20.95	0.04	0	0
13	112	559.5	120.9	-	-	-	-	100	-
14	112	337.7	28	-	-	-	-	100	-
15	134	138	22.96	-	-	-	-	100	-
16	16.0	299	3.52	-	-	-	-	100	-
17	150	32.2	0.048	-	-	-	-	100	-
18	9.6	230	28	-	-	-	-	100	-
19	160	32.2	1	-	-	-	-	100	13
20	1015	87	1	0.96	80.64	11.79	6.61	0	0

Total Power Output ($\dot{W}$)	**Net Electricity Efficiency**	**CO_2 emission**
454 MW	32.4 %	0.791 kg/kWh

3.2.3.2 Turbine Outlet Temperature reduced from Reference Case (Case 2b)

One possible way in which the SCC system of Case 2a can be improved is by lowering the turbine outlet temperature (TOT) of the gas-turbine to a value typical for a simple Brayton cycle; the lower TOT means higher work output from the turbine and therefore, more electrical power can be produced [25]. For example, in their simple Brayton cycle study, Abam et al. reported a TOT value of 457 ^{0}C, a value considerably lower than the 608 ^{0}C specified in the NGCC study of Manzolini et al. [20]. The energy balance calculations showed that changing the TOT to 457 ^{0}C, leads to an increased gas-turbine power of 366 MW, as reported in Table 3.6.

Because of the lower temperature in Stream 6, the rate of the ambient airflow in Stream 7, required for cooling, is also reduced (i.e., 146 kg/s compared to 265 kg/s in Case 2a). If the gas mixture in Stream 10 is mixed with 47 kg/s of additional ambient air coming from Stream 12, the Reference Case temperature of 608 ^{0}C is obtained for Stream 11, which has a total mass flow rate of 868 kg/s.

To match the HRSG temperatures from the Reference Case, a total inlet flow rate of water in Stream 19 is $\dot{m}_w$=131 kg/s, which is lower than 160 kg/s of inlet water in Case 2a. The power output from the HRSG in Case 2b is lower than in Case 2a due to the lower mass flow of water; however, the total power output from the SCC system increases from 454 to 531 MW. The thermal efficiency increases from 32.4 to 38.0 % and the CO_2 emissions are reduced from 0.791 to 0.675 kg/kWh, an improved value lower than the representative value for PC plants of 0.762 kg/kWh.

Table 3.6: Mass flow rates, pressure, temperature and composition of main streams of sulfur combined cycle with heat recovery from FGD in HRSG and a lower TOT (Case 2b).

Stream	$\dot{m}$	**T**	**P**	**Composition (% mol)**					
	(kg/s)	**(^{0}C)**	**(bar)**	**Ar**	**N_2**	**O_2**	**CO_2**	**H_2O**	**SO_2**
1	650	15	1	0.93	78.08	20.95	0.04	0	0
2	523	516	18.16	0.93	78.08	20.95	0.04	0	0
3	72.0	25	1.01	Elemental Sulfur (100 %)					
4	72.0	160	1						
5	595	1328 (COT)	17.6	0.93	78.08	8.50	0.04	0	12.45
6	722	457	1.1	0.93	78.08	10.92	0.04	0	10.03
7	146	15	1	0.93	78.08	20.95	0.04	0	0
8	225	15	1	Calcium Carbonate $CaCO_3$ (100 %)					
9	306	900	1	Calcium Sulfate $CaSO_4$ (100 %)					
10	787	900	1.06	0.97	81.41	9.04	8.58	0	0
11	868	608	1.04	0.97	81.22	9.73	8.08	0	0
12	47	15	1	0.93	78.08	20.95	0.04	0	0
13	92	559.5	120.9	-	-	-	-	100	-
14	92	337.7	28	-	-	-	-	100	-
15	110	138	22.96	-	-	-	-	100	-
16	13	299	3.52	-	-	-	-	100	-
17	124	32.2	0.048	-	-	-	-	100	-
18	7.9	230	28	-	-	-	-	100	-
19	132	32.2	1	-	-	-	-	100	13
20	868	87	1	0.97	81.22	9.73	8.08	0	0

Total Power Output ($\dot{W}$)	**Net Electricity Efficiency**	**CO_2 emission**
531 MW	38.0 %	0.675 kg/kWh

3.3 Summary of Results

The performance of the NGCC Reference Case, the SCC with no FGD heat recovery (Case 1) and the SCCs with FGD heat recovery (Case 2a and 2b) are compared in Table 3.7.

Table 3.7: Summary of Results for the Different Cases.

	Reference Case	Case 1	Case 2a	Case 2b
$\dot{m}_{Fuel}$, kg/s	15.3	72.0	72.0	72.0
TOT, ^{0}C	608	608	608	457
$\dot{W}_{Gas\ Turbine}$, MW	272	253	253	366
$\dot{W}_{HRSG}$, MW	138	90	201	166
$\dot{W}_{Total}$, MW	410	342	454	531
$\eta_{Gas\ Turbine}$ (LHV base), %	38.5	37.8	37.8	54.7
η_{Total} (LHV base), %	58.1	24.5	32.4	38.0
CO_2 emission, kg/kWh	0.360	1.045	0.791	0.675

The NGCC Reference Case shows a power generation efficiency of 58.1 %, comparable to the Reference NGCC plant of Manzolini et al. [20]. The predicted overall efficiency for the SCC with no FGD heat recovery, using the assumptions in Table 1, is 24.5 %. For the SCCs cases with FGD heat recovery, the power generation efficiencies are of higher values (i.e. 32.4 % in Case 2a and 38.0 % in Case 2b). All of the calculated SCC efficiencies are lower than the NGCC due to the lower combustion capacity of sulfur compared to NG in the gas-turbine. In Case 1, the energy recovery in the HRSG was restricted due to the redirection of a part of the available for the HRSG to heat the FGD; In Cases 2a and 2b, the FGD temperature was fixed at 900 ^{0}C due to reaction limitation at higher temperature, and therefore bounded the thermal energy that can be recovered in Cases 2a and 2b from the flue gas coming out of the FGD.

Compared to the total power output of the Reference Case (410 MW), Case 1 resulted in a lower power output value of 261 MW. Case 2a and Case 2b produced higher power outputs of 454 MW and 531 MW, respectively. The low power output computed for Case 1 is a worst-case value because the 126 MW_{th} required to maintain the FGD at 900 ^{0}C may be available as waste heat from another source.

Also, heat recovery from the hot FGD product "anhydrite" could have been a potential source of extra energy (calculated at 268 MW but not integrated in the efficiency). Cases 2a and 2b have markedly improved the power outputs because no external heat source for the FGD was required due to the higher temperature of the exit stream from the gas-turbine. The exit temperature from the gas turbine is lower in Case 2b compared to Case 2a, resulting in two effects: i) an increase in the gas turbine power output and ii) a decrease in the HRSG power output with the net result being a higher overall power output.

Another criterion considered in this study was the CO_2 emissions per kWh. Compared to the NGCC value of 0.36 kg/kWh, the SCC system with no FGD heat recovery (Case 1) produced a total of 1.045 kg/kWh, whereas the system with FGD heat recovery produced 0.791 kg/kWh when TOT was matched to the Reference Case, and an improved value of 0.675 kg/kWh when TOT was reduced to 457 ^{0}C. These values are comparable to a typical new PC plant that would emit 0.762 kg/kWh [24].

Overall, this study suggests that the Case 2b of SCC system with FGD heat recovery shows promise as an electrical power plant with lower CO_2 emissions than a PC plant.

3.4 Conclusions

This study compares three possible systems for electricity production from elemental sulfur using a natural gas combined cycle system as a Reference Case. In all three cases, the sulfur combustion unit and gas compressor/turbine system is combined with a flue gas desulfurization (FGD) unit and a heat-recovery steam-generator (HRSG) system. The first case considered had a relatively low efficiency because it does not consider energy recovery from the exothermic SO_2

conversion to anhydrite in the FGD unit. Cases 2a and 2b obtained improved performance by placing the FGD unit before the HRSG so that additional energy recovery can occur from the hot flue gas leaving the FGD. Case 2b is more efficient than Case 2a because more energy was recovered by the gas-turbine due to the lower turbine outlet temperature, and less extra air is used in FGD to achieve the specified operating temperatures. The CO_2 emissions from Case 2b were the lowest among the SCC cases considered. Although the CO_2 emissions are higher than from a comparable NGCC plant, they are lower than a typical modern PC plant.

This analysis is a step toward a longer-term goal of converting waste sulfur to benign anhydrite and electrical energy with low CO_2 emissions. Appropriate process design and optimization will be further required to determine whether increased efficiency of power production and reduced CO_2 emissions can be obtained compared to the values presented here. Further research is also required to obtain improved knowledge about any impediments (e.g. construction materials, reaction kinetics and achievable SO_2 emissions) to practical operation of this type of SCC system. Further criteria such as capital cost, hours of operation and the need for new technology development can be considered but are not presented in the current work.

3.5 References for Chapter 3

[1] U.S. Geological Survey. Mineral commodity summaries 2014-Sulfur. p 156.

[2] Canadian Minerals Yearbook (CMY) – 2009. Sulphur. Natural Resources Canada. Retrieved from: http://www.nrcan.gc.ca/mining-materials/markets/canadian-minerals-yearbook/2009/8470

[3] Song C. An overview of new approaches to deep desulfurization for ultra-clean gasoline, diesel fuel and jet fuel. Catalysis Today 86 (2003) 211–263

[4] Elsner MP, Menge M, et al. The Claus process: teaching an old dog new tricks. Catalysis Today 79–80 (2003) 487–494.

[5] Srivastava RK, Jozewicz W. Flue Gas Desulfurization: The State of the Art. Air & Waste Manage. Assoc. (2001) 51:1676-1688.

[6] Lee KS, Jung JH, et al. Characterization of calcium carbonate sorbent particle in furnace environment. Science of the Total Environment 429 (2012) 266–271.

[7] Furtes AB, Velasco G et al. Study of the direct sulfation of limestone particles at high CO_2 partial pressures. Fuel Processing Technology 38 (1994) 181-192.

[8] Katolicky J, Jicha M. Influence of the lime slurry droplet spectrum on the efficiency of semi-dry flue gas desulfurization. Chem. Eng. Technol. 2013, 36, No. 1, 156–166.

[9] Dam-Johanson K, Ostergaard K. High temperature reaction between sulphur dioxide and limestone-I. comparison of limestone in two laboratory reactors and a pilot plant. Chemical Engineering 46 (1991) No. 3, 827-837.

[10] Wang C, Jia L, et al. The effect of water on the sulphation of limestone. Fuel 89 (2010) 2628–2632.

[11] Chen J, Yao H, Zhang L. A study on the calcination and sulphation behaviour of limestone during oxy-fuel combustion. Fuel 102 (2012) 386–395.

[12] Laursen K, Duo W, et al. Sulfation and reactivation characteristics of nine limestones. Fuel 79 (200) 153–163.

[13] Siagi ZO, Mbarawa M, Mohamed ARet al. The effects of limestone type on the sulphur capture of slaked lime. Fuel 86 (2007) 2660–2666.

[14] U.S. Geological Survey. Mineral Commodity Summaries 2014-Gyspum. p.70.

[15] U.S. Geological Survey. Gypsum (2001). Prepared by Olson DW.

[16] U.S. Geological Survey. Mineral commodity summaries 2014-Sulfur. p 156.

[17] Rappold TA, Lackner KS, Large scale disposal of waste sulfur: From sulfide fuels to sulfate sequestration, Energy. 35 (2010) 1368-1380.

[18] Gas Turbine World, 2009. Handbook.

[19] Horkeby K. Simulation of Heat Recovery Steam Generator in a combined cycle power plant. Linkopeng 2012.

[20] Manzolini G, Macchi E, et al. Integration of SEWGS for carbon capture in natural gas combined cycle. Part B: Reference case comparison. International Journal of Greenhouse Gas Control 5 (2011) 214–225.

[21] Amrollahi Z. Optimized process configurations of post-combustion CO2 capture for natural-gas-fired power plant – Power plant efficiency analysis. International Journal of Greenhouse Gas Control 8 (2012) 1–11.

[22] Meyer B. Elemental Sulfur. Chemical Reviews. 76-3 (1976).

[23] García-Labiano F, Rufas A, et al., Calcium-based sorbents behaviour during sulphation at oxy-fuel fluidised bed combustion conditions, Fuel. 90 (2011) 3100-3108.

[24] IPCC, 2005: IPCC Special Report on Carbon Dioxide Capture and Storage. Prepared by Working Group III of the Intergovernmental Panel on Climate Change [Metz, B.,O. Davidson, H. C. de Coninck, M. Loos, and L. A. Meyer (eds.)]. Cambridge University Press, Cambridge, United Kingdom and New York, NY, USA, 442 pp.

[25] Abam DPS, Moses NN. Computer simulation of a gas turbine performance. Global Journal Inc. 11-1 (2011).

[26] Smith JM, Van Ness HC. Introduction to Chemical Engineering Thermodynamics. 4th Ed. McGraw Hill.

[27] Haynes WM, Lide DR, D. R. CRC handbook of chemistry and physics: A ready-reference book of chemical and physical data- Chapter: Standard thermodynamic properties of chemical substances. Boca Raton, Fla.

Chapter 4

Development of Lab-Scale Reactor Systems and Experimental Studies of Sulfur-Calcite Reactions

This chapter studies the lab-scale production of anhydrite from calcite, sulfur and oxygen through the overall reaction (R4.1):

$$CaCO_3(s) + S(s) + 3/2\,O_2(g) \rightarrow CaSO_4(s) + CO_2(g) \qquad \Delta H^0 = -620.4\ kJ/mol \qquad \text{(R4.1)}$$

The study performed used three different experimental setups: In the first, sulfur and calcite were placed together in a Thermogravimetric Analysis (TGA) apparatus with oxygen, air or nitrogen atmosphere. The second setup was a lab-scale reactor where sulfur was gasified in the presence of oxygen in one vessel and then contacted with calcite in a second vessel. In the third setup, sulfur and calcite solids were placed in the same vessel in an air or oxygen environment and reacted. The two last setups were new lab-scale reactors designed and built as part of this thesis.

TGA was performed on reactants and product samples to characterize their thermal behavior and make inferences about composition. X-ray microanalysis was also performed to identify components in the samples.

4.1 Materials Used

The chemicals used in the experiments were:

- Calcite ($CaCO_3$) provided by Acros Organics, >99% pure
- Natural limestone provided by Lafarge Inc, containing calcite and raw minerals
- Sulfur (S) provided by Fischer Scientific; 100% pure
- Calcium Oxide (CaO) provided by Fischer Scientific; >99.8 % pure
- Calcium Hydroxide ($Ca(OH)_2$) provided by Fischer Scientific; >99 % pure

Gases used in the experiments, were all provided by Air Liquide ^{LTD} and included pure N_2, O_2, CO_2 and "bone dry" air.

4.2 Thermogravimetric Analysis (TGA) for Mixtures of Reactants

4.2.1 TGA of Limestone and Sulfur in N_2 and Air

In the first set of experiments, limestone and elemental sulfur were mixed in different ratios to test for potential reaction when the mixture is heated in a TGA apparatus. The TGA apparatus used was a TA instruments Q50 model provided in the Royal Military College of Canada laboratories. The experiments were conducted as follows: at the beginning of every run, the initial mass of the platinum sample pan was tared under a N_2 atmosphere. Then, around 15 mg of the sample to be tested was spread on the pan. The pan was automatically hooked into the balance and the furnace was closed. The sample temperature was ramped to the required temperature of 850 ^{0}C with a heating rate of 20 ^{0}C/min.

The compositions of the samples tested were set at 75-25 %, 86-14%, and 90-10% of limestone and sulfur. The mixture of 75 % limestone and 25 % sulfur showed a first mass drop between 200 ^{0}C and 300 ^{0}C; the mass of the sample stayed constant until 600 ^{0}C and then started dropping

again in the 600 to 800 ^{0}C range. As shown in Figure 4.1, this behavior was seen in N_2 flow at 40 mL/min and in air atmosphere at flow rates of 10 and 40 mL/min. The figure shows the mass drops in solid lines, and the rate of weight change in dashed lines. The first mass drop that occurred was of 25.8 % with a peak at 270 ^{0}C. The size of the first mass drop, which corresponded to about the total mass of sulfur, suggested that all sulfur was gasified and did not react with calcite found in limestone. The second mass drop at around 740 ^{0}C showed a drop of 24 % and was suggested to be due to the calcination of $CaCO_3$ found in limestone.

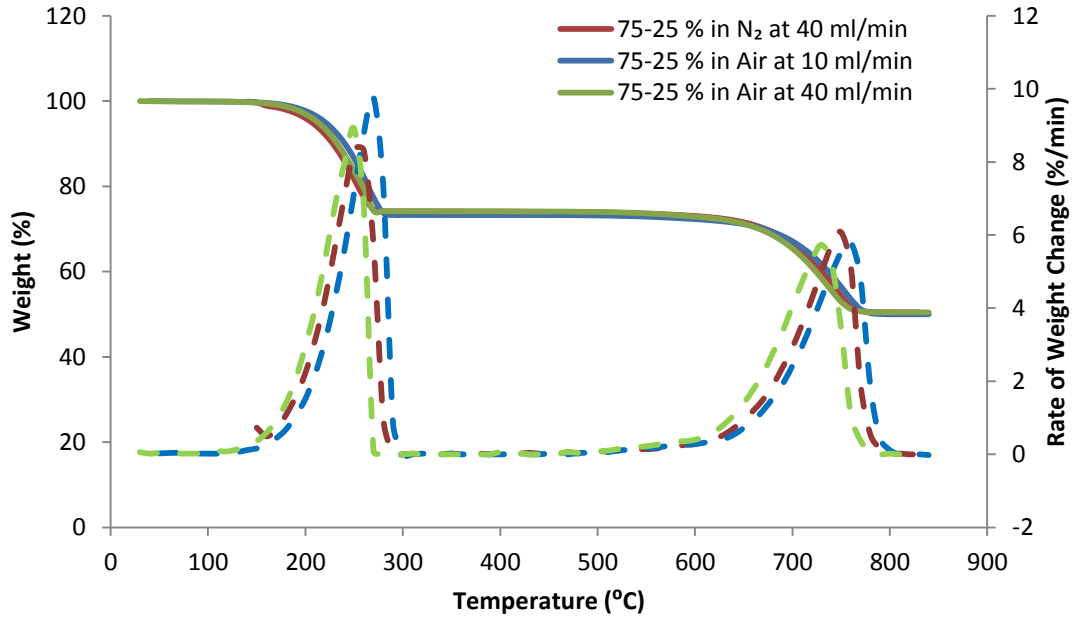

Figure 4.1: Mass drop in function of temperature for 1:1 molar ratio mixture of limestone and sulfur. Solid lines correspond to the "Weight" axis and the dashed lines correspond to the "Rate of Weight Change" axis.

Similar behavior was also found in the two other mixtures, where the first mass drops corresponded to the total mass of sulfur and the second corresponded to the mass change expected when calcite decomposed to form CaO and CO_2. The first mass drop was 14 % for the 2nd Limestone-S mixture and 10 % for the 3rd mixture corresponding both to the total sulfur mass.

In follow-up experiments, TGA of pure sulfur showed a total mass loss between 200 and 300 ^{0}C in air and nitrogen atmosphere (see Figure 4.2). A note that the TGA curve for pure sulfur in air atmosphere showed a bump in the curve at 300 ^{o}C; the suggested explanation was the exothermic reaction between sulfur and oxygen in the air increasing suddenly the temperature, and therefore resulting in a faster loss of mass. Plotting the curve of 'temperature' vs 'time' shows a sudden increase in temperature from 300 to 360 ^{o}C at the minute 15, instead of a continuous 20 ^{o}C/min slope (equal to the heat rate) confirming the exothermic reaction hypothesis. Note that this did not occur in the limestone-sulfur mixture because of the smaller total amount of sulfur in the pan.

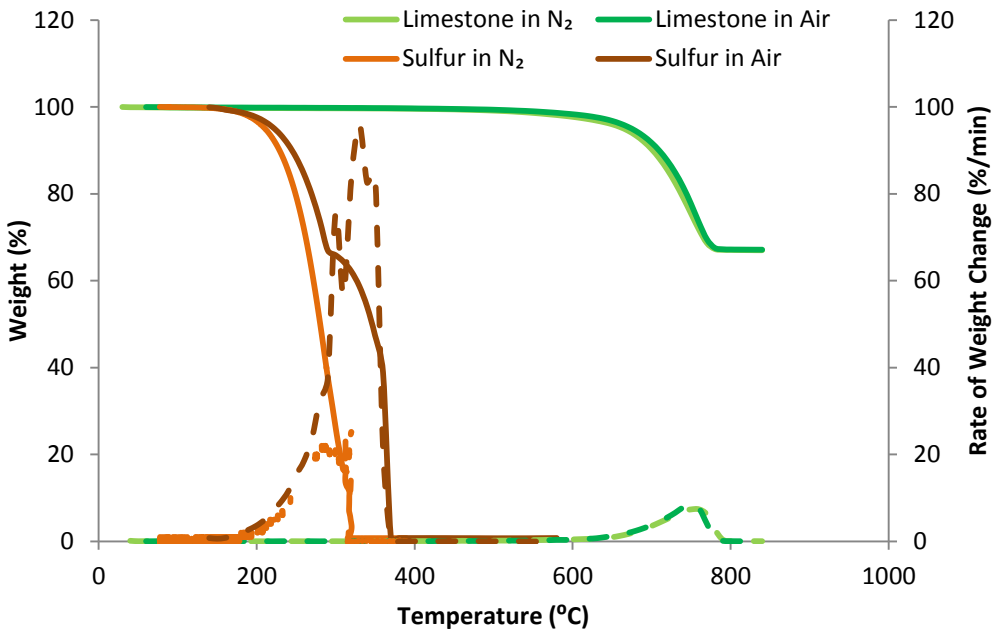

Figure 4.2: Mass drop in function of temperature for a pure sulfur sample and a limestone sample. Solid lines corresponds to the "Weight" axis; Dashed lines for the "Rate of Mass Change".

As for the TGA of limestone, the mass loss was of 33 % between 600 and 800 ^{0}C. In Figure 4.1, the second drop corresponds to the conversion of calcite part of limestone to lime (CaO); it was

equal to 75 % x 33 %, since the mixture of limestone-sulfur was 75-25 % and, therefore, the second mass drop was around 24 %.

As a result of these findings, it was suggested that when sulfur and limestone are mixed at various ratios, under air atmosphere at a 40 ml/min flow rate, sulfur gasifies in the 200-300 ^{0}C range leaving the furnace of the TGA without any reaction with limestone, which calcines alone above 600 ^{0}C.

4.2.2 TGA of Equimolar Calcite-Sulfur Mixture in N_2 and O_2

In another set of experiments, calcite and sulfur were mixed at a 1:1 molar ratio and tested for potential reaction when heated in the TGA apparatus, with a flow of pure oxygen instead of air. The tests were performed first with a flow of pure nitrogen for comparison, then with a flow of pure oxygen, at 60 ml/min. The TGA experiments showed that when heated from room temperature to 850 ^{0}C, under pure nitrogen flow, two mass drops occurred, one in the 200-300 ^{0}C range, and the second in the 600-800 ^{0}C range. The corresponding Figure 4.3 shows that under N_2 atmosphere flowing at 60 ml/min, the first mass drop was 25 %, equal to the total mass of sulfur present in the sample; and the second drop was 32 % corresponding to calcination of $CaCO_3$ to CaO. The values of the two drops suggested that all sulfur has gasified before any reaction with calcite, as expected from previous experiments with limestone.

However, when switched to a pure oxygen environment at a 60 ml/min flow, the first mass drop reached 21.85 % instead of 25 %, suggesting that not all of sulfur gasified and that 13 molar % of the sulfur stayed in the pan. In addition, the drop related to the calcination of $CaCO_3$ had a value

of 24.17%, in O_2 flow, lower than that in N_2 suggesting that not all $CaCO_3$ has calcined to CaO, as shown in Figure 4.3.

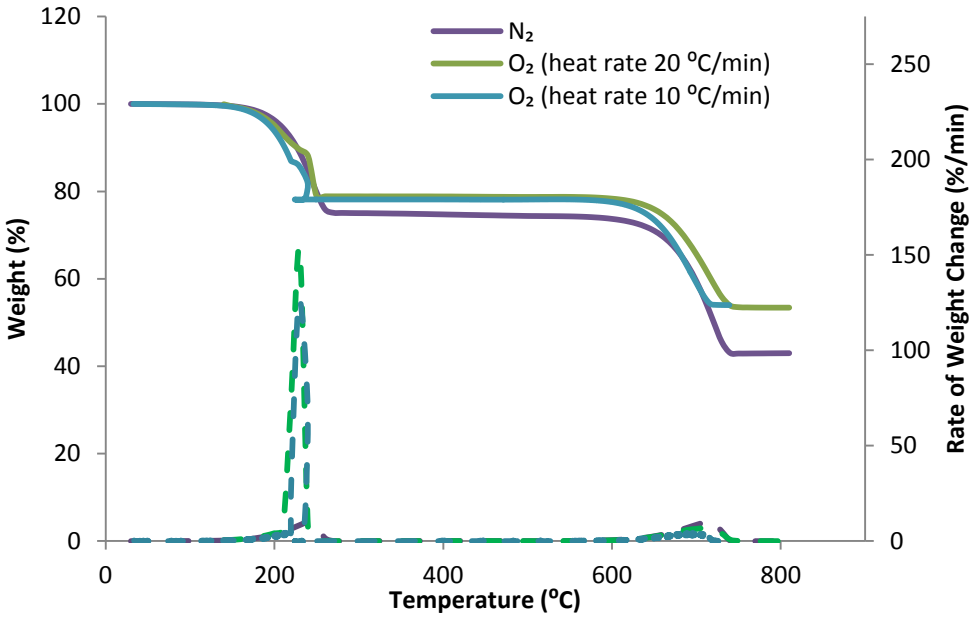

Figure 4.3: Mass drop in function of temperature for 1:1 molar ratio mixture of calcite and sulfur in pure N_2 and O_2. Solid lines corresponds to the "Weight" axis; Dashed lines for the "Rate of Weight Change".

An explanation of the lower mass drops can be that a reaction between calcite, sulfur and oxygen occurred to produce $CaSO_4$; the product $CaSO_4$ weighs 3 % more than the $S/CaCO_3$ mixture (due to addition of a mole of oxygen minus the loss of a mole of C) and would result in an increase in the mass if all the sulfur and calcite have reacted when mixed in equimolar ratios. The smaller drop in mass for $CaCO_3$ (100 g/mol) suggested that 82 molar % calcined to CaO (56 g/mol), while the 18 % left was suggested to be converted to the higher mass $CaSO_4$ (136 g/mol). This value is higher than the 13 molar % of sulfur that remained in the pan and did not gasify, suggesting that only 13 % of $CaCO_3$ converted to $CaSO_4$ (since the mixture is equimolar), leaving 5 % potentially unreacted due to the formation of the product $CaSO_4$ on the surface.

To make sure that the heating rate does not affect the value of the mass drop, two heating-rate values were used, 10 ^{0}C/min and 20 ^{0}C/min, with the same oxygen flow; the mass drop was the same for both heating rates and the only difference was that the drop in mass for calcite was achieved 10 ^{0}C earlier at the lower heating rate.

The results of this section suggested that in a TGA apparatus, in the best case scenario, only 13 % of sulfur was converted to anhydrite when pure oxygen was used. The sulfur is mostly gasified starting at 200 ^{o}C and escapes from the furnace before satisfactory long contact occurs with calcite at higher temperatures.

4.3 Two-Vessel Reactor for Sulfur-Calcite Reaction

Conducting the sulfur-calcite reaction in a TGA apparatus was hard to achieve due to escape of gaseous sulfur from the pan before significant reaction with calcite could occur. Therefore, a lab-scale reactor was built in a laboratory at Royal Military College of Canada to conduct more thorough experiments that allow contact between sulfur and calcite at high temperatures. The apparatus was located in a fume-hood for safety purposes, thereby preventing emission of sulfur fumes into the lab. The apparatus consisted of two main parts, a sulfur evaporator to the right and a reactor the left, as shown in Figures 4.4.

Figure 4.4: Lab-scale sulfur evaporator and sulfur-calcite reactor in RMC laboratory.

4.3.1 Experimental Design of the Apparatus

The reactor was a stainless steel tube of 45 cm height; while the sulfur evaporator, made also from stainless steel, was a smaller 22 cm tube, and welded closed at the bottom. Both tubes had a 25.4 mm inside diameter, and a thickness of 1 mm. The middle of the reactor was fitted in a cylindrical ceramic heater of 23 cm height; while the evaporator was inserted through the top of a ceramic oven. A diagram of the system is shown in Figure 4.5. The ceramic heater was connected to a temperature controller, while the ceramic oven had a built-in controller. The two vessels were connected by stainless-steel ¼ in. tubes that are either rigid or flexible depending on their location. A three-way valve connected the feed of gas to the evaporator, or by-passed the evaporator so that the gas flows directly to the reactor. A one-way valve (shown in red) was inserted at the exit tube of the reactor to prevent backflow of gas from top to bottom, while a second one-way valve, inserted at the exit tube of the evaporator, prevented flow of gas back to

the evaporator. Heat tape was wrapped around all the stainless steel tubes to heat the gas flowing between the vessels. The tape was covered with glass wool to reduce heat transfer.

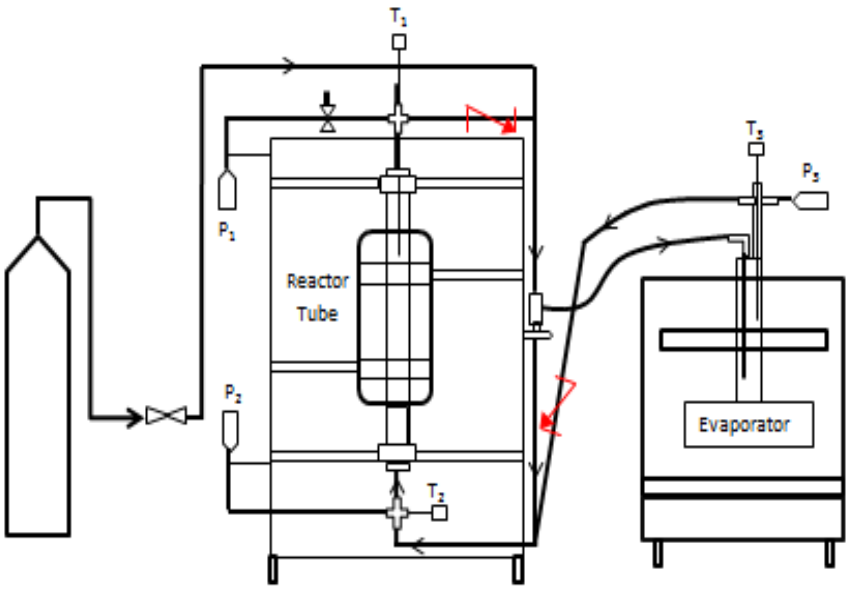

Figure 4.5: Diagram of the lab-scale sulfur evaporator and sulfur-calcite reactor.

An Omega® type K dual-thermocouple was inserted through the top of the reactor. It was connected to the Omega® auto-tune PID temperature controller through one outlet, and to a Natural Instrument (NI) compactDAQ module through the other. The module interfaced temperature measurements with NI LabVIEW software on a computer through the NI compactDAQ chassi and a USB connector. Other thermocouples were also installed at the bottom of the reactor and the top of the evaporator, and connected to the same NI module. Pressure transducers were connected to the top and bottom of the reactor and the top of the evaporator, and were used to send pressure data to another NI compactDAQ that reads voltage measurements.

Note that in earlier stages of the design, the two vessels material was chosen to be quartz glass; however, the vessels were easily chipping and therefore, substitution to stainless steel tubes was necessary. Swagelok® fittings were used at the top and bottom of the reactor and the top of the evaporator to connect the ends of the vessels to the smaller-size connecting tubes.

Many primary runs were performed before any experiments with reactants occurred. Then, some experiments were run with calcite, sulfur or a mixture of both under nitrogen atmosphere, before the required experiments under oxygen environment were started.

4.3.2 Experimental Procedure

At the beginning of each experiment, the fittings on the ends of the reactor and the one on top of the evaporator were opened using a wrench to enable removal of the vessels from the heaters and load the solid samples. The calcite sample was inserted in the reactor between two quartz wool plugs; the wool held the sample in the middle of the tube. In the evaporator, sulfur was inserted and covered with quartz wool to prevent the sample from being carried out of the vessel by the flowing gas. Once the samples were in place, the vessels were inserted back into the heaters and the fittings were closed. At the start of each experimental run, Superwool® was inserted between the ceramic heater and the reactor to reduce heat loss. Similarly, Superwool® was wrapped around the evaporator at the top of the oven. Using the temperature controller connected to the dual thermocouple on top of the reactor, the setpoint temperature was reached through an Omega PID controller with auto-tuning. The controller allowed heating to the required temperature in a short time period (typically ~15 min.) with minimum overshoot. Once the required temperatures in the reactor and the evaporator were reached, the gas valve was opened and oxygen was flowed to the evaporator. The feed valve of oxygen was then closed and the valve between the two vessels was opened allowing the mixture of gasified sulfur and oxygen to pass through the tubes and enter the

reactor from the bottom, to react with the bed of calcite. The gas source and exit valves were then opened together to allow a continuous flow of oxygen through the evaporator and reactor. After oxygen has flowed to the vessels, the feed valve was closed and the run was terminated. The controllers were turned off and Superwool® between the heater and the vessels was removed to allow faster cooling. The vessels were opened, quartz wool was removed from the upper fitting and the reacted calcite sample was poured into a sampling jar.

The conditions of experiments in this apparatus were varied as follows: the setpoint temperature in the reactor was varied in the range of 700 to 900 ^{0}C at intervals of 50 ^{0}C, while the evaporator was heated to 500 ^{0}C in all experiments, a temperature high enough to make sure that all sulfur was gasified and potentially oxidized. The mass of calcite was fixed at 1.0 gram; while the sulfur mass was varied between 1.0 and 2.0 grams (x 3 or x 6 times the equimolar amount required). The sulfur amounts chosen were in excess as to ensure that sufficient sulfur was available for reaction. The gas used in these experiments was always oxygen.

The objective of these experiments was to investigate the reaction of sulfur with calcite and oxygen in the given conditions of mass ratios and temperature range.

4.3.3 Testing Method and Results

To test for the composition of the reacted samples, Energy Dispersive X-ray Spectroscopy (EDS) tests were performed on the collected samples using an AMETAK® instrument equipped with a Scanning Electron Microscope (SEM) and a TEAM™ EDS analysis system, provided in the RMC laboratories. Figure 4.6 shows the peaks corresponding to the elements present in one of the samples. The elements observed were Ca, S, O and C. For the various conditions of temperature and sulfur mass, the same four elements were detected, but their relative amounts varied as shown in Table 4.1. The carbon amounts were negligible and therefore not shown in the table.

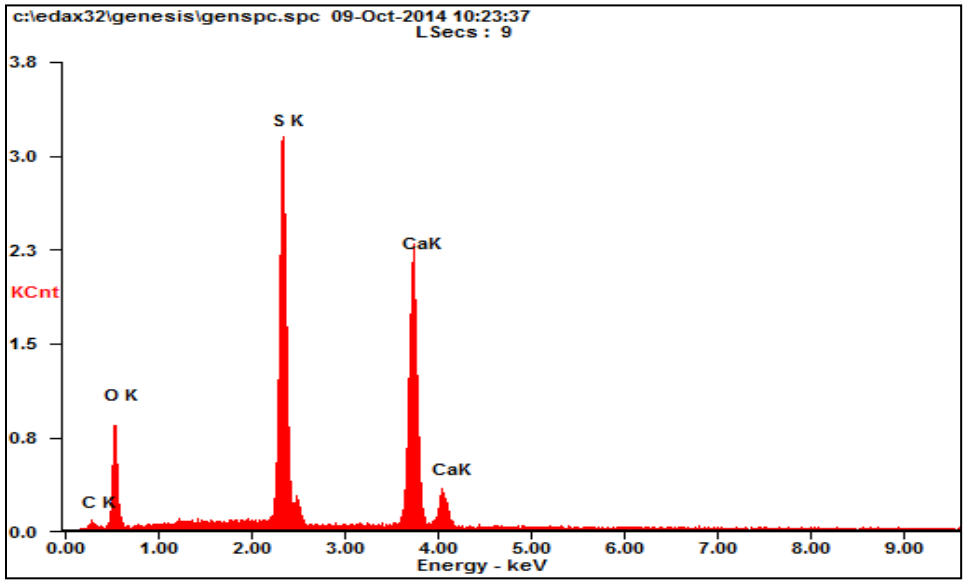

Figure 4.6: EDS spectrum showing the presence of Ca, S, O and C elements.

Table 4.1: EDS results for solid residue from first reactor setup. Theoretical 100% reaction values: 16.7 % Ca/ 16.7 % S/ 66.6 % O by mole.

Sample #	Temperature (^{0}C)	Mass of Sulfur (g)	% Ca	% S	% O
1	700	1.0	20.1	17.1	61.8
2	750	1.0	27.9	19.4	51.7
3	800	2.0	18.1	13.7	68.2
4	850	1.0	16.7	16.7	66.6
5	850	2.0	17.5	16.3	66.2
6	900	1.0	18.4	14.3	67.3
7	900	2.0	15.7	15.7	68.6

4.3.4 Analysis of the Experimental Results from the First Setup

The presence of the element sulfur in all of the reacted calcite samples suggests that some fraction of calcite reacted with sulfur to produce a compound containing sulfur. In samples 4 and 7, the

molar percentages of Ca and S were found to be equal; and the molar amount of oxygen was around 4 times that of S or Ca. This distribution of molar percentages among the elements suggests that the only compound present at appreciable concentration in samples 4 and 7 was $CaSO_4$, identified by the equimolar amount of sulfur and calcium, and an oxygen amount four times that of calcium. In the other samples, the sulfur amount was lower than calcium suggesting that not all of the calcite reacted with sulfur and that some of it is still present in the CaO form. Assuming that an equal amount of S and Ca minerals means total conversion of calcite to anhydrite, the ratio of S to Ca can give an estimate of the percentage of conversion. The results are shown in Figure 4.7.

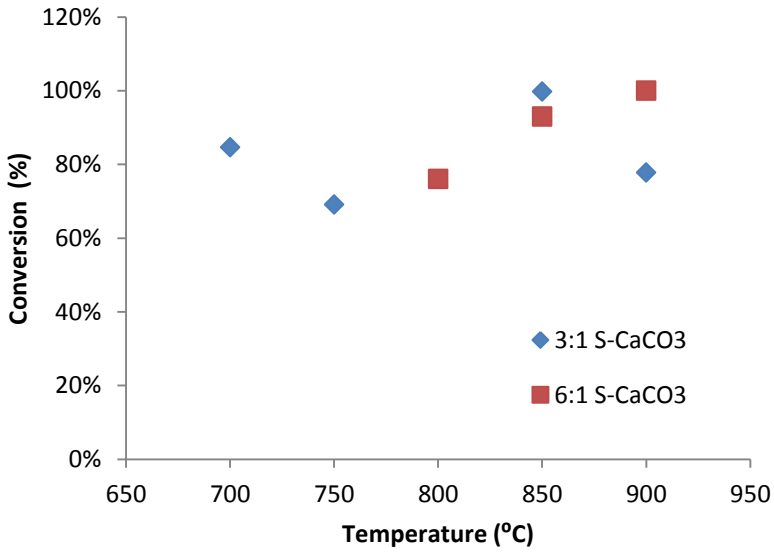

Figure 4.7: Results of first lab-scale sulfur-calcite reactor for 3:1 and 6:1 molar ratio of Sulfur to Calcite.

The lowest conversion percentage was 69 % at a temperature of 750 ^{0}C when 1.0 gram of sulfur was used (> 3:1 molar ratio of S-$CaCO_3$); 100 % conversion was achieved at 850 ^{0}C for the same molar ratio, and at 900 °C for the 6:1 molar mixture. While Figure 4.7 does not show a direct

relationship between conversion and temperature for the 3:1 S-$CaCO_3$ experiments, it does show a trend for the experiments with 6:1 molar ratio of S-$CaCO_3$, where the conversion increased from 76 to 100 % when the temperature of experiment increased from 800 to 900 ^{0}C. The trend line might have been different if experiments at the lower 700 and 750 °C temperature were available.

At the end of the experiments, some sulfur was found accumulated in the tubing between the evaporator and reactor; the lower temperature (~100 ^{0}C) in the connecting tubes could be the reason for this sulfur condensation, resulting in variation of the amount of sulfur reaching the reactor. To eliminate the effect of having condensation on the connecting tubes, it was decided to move sulfur into the reactor in subsequent experiments.

In conclusion, this section was important to help understanding the apparatus and verify the possibility of producing anhydrite starting with elemental sulfur, calcite and oxygen. The tests suggested the capacity of full conversion of calcite to anhydrite at temperatures of 850 and 900 °C.

4.4 Modified Lab-Scale Apparatus for Sulfur-Calcite Reaction

To achieve a better reaction between sulfur and calcite and to prevent the condensation of sulfur on the inner surface of the connecting tubes, the experimental design was changed and a new set of experiments was performed. In this part of the study, the reactor was used without the evaporator and the feed of gas was directly flowed to the bottom of the reactor. Sulfur and calcite were both inserted in the reactor; sulfur was spread on quartz wool in the bottom of the reactor, while calcite was held by quartz wool in the middle.

In these experiments, the variables changed were: the ratio of sulfur to calcite, the setpoint temperature, and the gas used. The molar ratio of sulfur to calcite was varied between 0.5:1, 1:1,

2:1 and 3:1. For the fixed 1.0 gram mass of calcite, the mass of sulfur added was changed between 0.16, 0.32, 0.64 and 0.96 g. The 0.5:1 molar ratio runs were added to show the effect of having excess of calcite compared to sulfur. In the 2:1 and 3:1 experiments, sulfur will be the reactant in excess; the tests in the previous section suggested that full conversion of calcite to anhydrite when S-$CaCO_3$ molar ratio was 3:1 is possible, resulting in no need to increase the ratio to a higher value of 6:1. The setpoint of the temperature controller was broaden to a wider range and varied between 600, 700, 800 and 900 ^{0}C with a 100 ^{0}C gap. The reason for the lower temperature 600 ^{0}C is to find the lower boundary at which the kinetics of reaction are explicitly unfavorable. The temperature was not increased beyond 900 ^{0}C knowing that it is a high enough temperature to calcine all of the $CaCO_3$ to CaO independently of CO_2 concentration. Experiments were conducted using both air and pure oxygen. The previous section showed that reaction occurred with pure oxygen atmosphere; however, more practical condition in industry would require an air atmosphere, therefore, reaction with oxygen found in air, was necessary to be compared with reaction with oxygen from a pure flow. The three variables resulted in a total of 4x4x2 = 32 runs.

The procedure for a typical experimental run is as follows: desired masses of sulfur and calcite were introduced in the tube at the bottom and middle of the tube on quartz wool. The tube was placed inside the heater and the Swagelok® fittings were closed. Superwool® was then placed in the gap between the tube and the heater. The controller was set to the desired temperature and turned on. Once the desired temperature in the center of the reactor was reached, the gas valve was opened and the gas flows from the bottom to the top resulting in an increase of the pressure within the tube to the regulated gas pressure, as long as the exit valve was closed. The exit valve was then opened for around 60 s, during which an increase in the temperature occurs for a few seconds, reflecting the possible occurrence of a spontaneous exothermic reaction. A drop in

temperature occurs as the flow of the cold gas continues. Once the gas valve is turned off, the temperature controller regulates the temperature back to its setpoint. The real-time values of temperature and pressure were shown instantaneously on the NI LabVIEW screen providing information about when the setpoint temperature is reached to turn on the gas inlet valve, and turn it off once an increase in temperature occurs. Once the experiment was completed, the temperature controller was turned off and the data recording was stopped. Cold air was then blown between the reactor and the heater to cool down the exterior temperature to a safe value. The reactor was then removed from the heater. The top fitting is opened and quartz wool was removed from the inside using tweezers and the reacted calcite sample was collected in a sampling jar labeled with the date and the conditions of the run. No yellow solid was found remaining on the quartz wool, suggesting that the sulfur sample was properly gasified during the runs. The process was repeated for the different variable combinations until the complete sample matrix was collected. An example of the NI LabVIEW temperature and pressure profiles is shown in Figure 4.8.

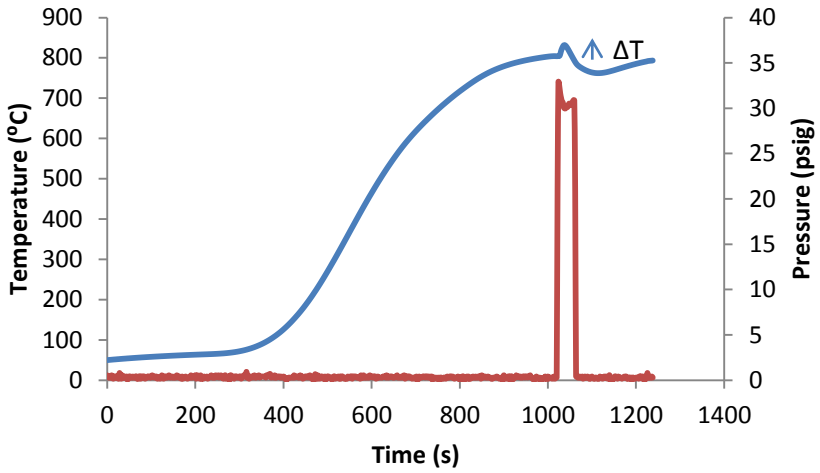

Figure 4.8: Temperature and pressure change during the experiment run of 2:1 calcite to sulfur ratio, reaching 800 ^{0}C under air atmosphere.

The example corresponds to a run with 1.0 g of calcite and 0.16 g of sulfur (0.5:1 S-$CaCO_3$ molar ratio), heated to 800 ^{0}C, in air atmosphere. The figure shows the rise in temperature to the desired setpoint of 800 ^{0}C. Once the setpoint temperature was reached, the gas valve was opened at 1022 s, resulting in a slight increase in temperature and a pressure of 30 psig.

Both oxidation of sulfur and sulfation of calcite are exothermic reactions; therefore, the slight increase in temperature ΔT can be attributed to the combination of these two reactions. After 42 s, the temperature started to drop again and that is when the gas inlet valve was closed and the purge valve was opened, dropping down the pressure back to 0. The temperature controller regulated the temperature back to 800 ^{0}C and the experiment was then terminated.

The increase in temperature after the flow of the gas, due to the exothermic reaction, varied in value between the different experiments and its value was shown in Figure A.1 in the Appendix in function of reactant ratio for gases and temperatures. The ΔT was almost always lower for the 0.5:1 and 1:1 reactant ratio and higher for the 2:1 and 3:1 reactant ratio experiments.

During the experiments, several additional factors varied between the runs. These factors were heating time required to reach the setpoint temperature, gas pressure and duration of gas flow. In the 32 experiments, the time for heating to the setpoint averaged around 18 minutes for the runs in which the temperature setpoint was 600, 700 and 800 ^{0}C; however, for the 900 ^{0}C runs, the average time of heating was around 28 minutes due mostly to the increased time for the controller to settle at the setpoint temperature. The time for which the gas flowed into the reactor averaged around 60 seconds but wasn't fixed at the same exact value. The time of the flow was changed if an early (or late) increase in the temperature occurred due to the occurrence of the exothermic reaction. The average of the gas pressure was 26.5 psi with a standard deviation of 10 psi. In addition, the reactor used was changed half-way through the experiments; the second reactor had

the same dimensions as the first, however, the Swagelok® fittings were replaced by bolted flanges because the threads on the Swagelok® fittings warped due to repeated twisting. The updated reactor design with the flanges is shown on the left in Figure 4.9. The flanges were more practical in opening as they required using a screwdriver to twist the hexagon-socket head screws instead of using a 1 in. wrench for the Swagelok® fitting that resulted in fusing of the threads.

Figure 4.9: Reactor 1 with flanges on the left and the other with Swagelok fitting.

4.5 XRD Analysis

To identify the components in the samples, X-Ray Diffraction (XRD) tests were run. The tests took place in the Geological Science Department at Queen's University. The apparatus used was an auto-sampler Philips X'Pert Pro MPD diffractometer. The machine is equipped with a cobalt tube that has a radiation wavelength of 1.789 Å. The tube power was set at 45 mA and 40 kV. The divergence slit used was of ¼ rad, which is half the angle of the anti-scatter slit of ½ rad. The radiation angle started at 2θ equal to 10 rad and ended at a 110 rad position. The time for step

measurements was 70 s/step. The diffraction patterns were recorded using X'Pert Data Collector software and analysis of the radiation peaks was performed in X'pert HighScore Plus.

The XRD tests were performed as follows: the samples were crushed to fine powder using a graphite mortar and pestle. Three sample holders were available for use: two different sizes of metallic 'backpack' holders for large or medium-sized samples, and oriented glass mount disks for smaller samples. The 32 samples that were tested were split between the large backpack holders and the oriented glass holders as they both require the same divergence slit and anti-scatter slit angles. For the samples mounted on the large sample holders, it was necessary to make the surface of the sample smooth for good x-ray diffraction on the surface. For the glass sample holders, the powder was rinsed with methanol after placement on the glass to allow random orientation of the powder. The samples were split randomly between the two types of holders to prevent a bias error due to the choice of the holder. In addition, one of the samples was tested in both types of holders and showed the same results regarding the composition. Note that the samples were split between the two types because not enough holders of the same size were available to run all 32 samples. The samples were mounted in the machine and the scanning was performed.

Using the X'Pert HighScore Plus program, the minerals in the samples were identified by matching the peaks to suggested minerals from the archive. Figure A.2 in the appendix shows an example of an x-ray profile where the components matching the peaks were calcite ($CaCO_3$), quick lime (CaO) and anhydrite ($CaSO_4$). Some of the samples showed additional presence of calcium sulfide (CaS), less commonly sulfur (S_8) and one sample showed the presence of $Ca(OH)_2$, as shown in Table A.1 in the appendix. The method used was a semi-quantitative analysis of the diffractogram based on the Reference Intensity Ratio (RIR); a more complex

quantitative analysis through XRD is the Rietveld method that requires more information about the crystalline structure and iteration of the instrumental parameters.

4.6 Thermogravimetric Analysis for Experimental Samples and Various Reactants

4.6.1 TGA for Reactants

In addition to XRD tests, TGA was performed on the samples to give a more quantitative evaluation of the components present in samples. Before testing the reacted samples through TGA, it was necessary to understand the thermal behavior of each of the reactants and products to compare the mass variation of the samples to a reference. TGA experiments were performed on commercial calcite, sulfur, quick lime, and hydrated lime.

The sample temperature was ramped to the required temperature of 950 ^{0}C with a heating rate of 20 ^{0}C/min. A note that additional tests with lower heating rate were performed to show the effect of changing the heating rate; lower heating rate can advance the drop in mass to slightly lower temperature but does not change the value in the final mass drop. The tests were performed under either pure N_2 or pure CO_2 atmosphere. The reason for using CO_2 atmosphere is to test for the presence of CaO. CaO is thermally stable in N_2 atmosphere as cited in Chapter 2; therefore, to test for its presence, CO_2 is introduced to carbonate CaO to $CaCO_3$ and test quantitatively for its amount. The behavior of the other pure components under CO_2 atmosphere also required testing to determine whether their thermal behavior would alter under the conditions of CO_2. The weight change for different components is shown in Figure 4.10 as a function of temperature. For elemental sulfur, the TGA experiment showed a drop in mass from 100 to 0 % in the temperature range between 200 and 330 ^{0}C showing that if sulfur existed in a mixed sample, it would gasify in this range for both N_2 and CO_2 atmospheres.

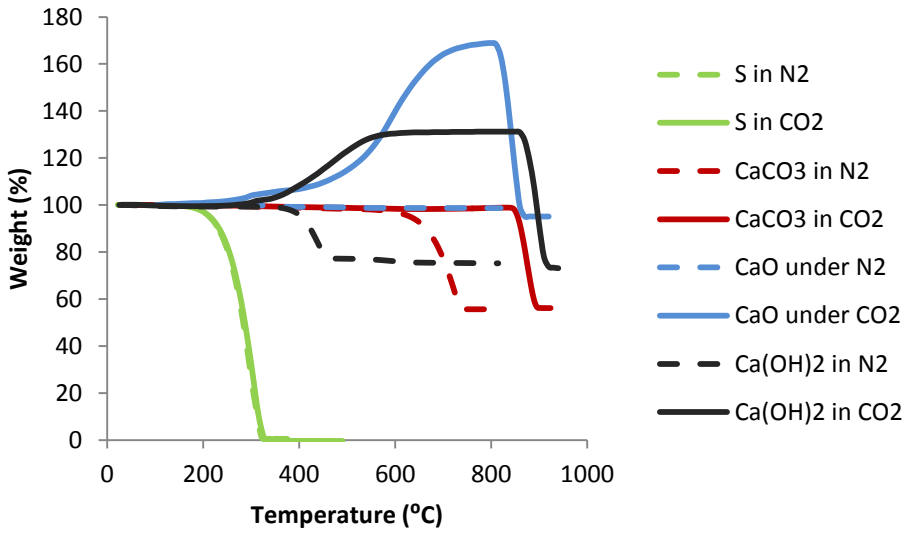

Figure 4.10: Mass vs temperature behavior of $CaCO_3$, CaO, $Ca(OH)_2$ and S in N_2 and CO_2 atmospheres.

Calcite ($CaCO_3$) dropped in mass to 56 % in the 600-700 ^{0}C range, in N_2 atmosphere. This is in agreement with the literature cited in Chapter 2, which indicates that $CaCO_3$ (100 g/mol) decomposes to CaO (56 g/mol) and CO_2 (44 g/mol) in this range through Reaction R2.3. In CO_2 atmosphere, calcination did not occur in the 600-700 ^{0}C range; instead, a sudden mass drop occurred in the 850-900 ^{0}C temperature range. This behavior is due to the CO_2 atmosphere in which calcination is prevented until a high temperature of ~900 ^{0}C is reached. At this temperature, calcination occurs independently from CO_2 concentration as cited in references discussed in Chapter 2. Although the mass drop in N_2 and CO_2 atmospheres occurred in different temperature ranges, the final mass of $CaCO_3$ samples was the same and equal to 56 %, which corresponds to the mass fraction of the CaO contained therein.

As for CaO, its thermal behavior in N_2 atmosphere is stable as cited in the references discussed in Chapter 2, and confirmed in Figure 4.10. The increase in the mass of CaO in CO_2 atmosphere is

related to the reverse reaction of R2.3 where CaO reacts with CO_2 and produces $CaCO_3$; the increase in the mass should theoretically reach 178 % (equal to 100 g/mol $CaCO_3$ divided by 56 g/mol CaO); however experiments showed that the final mass was up to 168 % of the initial sample mass. Additional tests were performed where the temperature in the TGA was fixed at 750 ^{0}C for 7 min. to test for any additional increase in mass; however, no additional increase occurred, presumably due to the sintering of the sample, which prevented CO_2 from reaching the particle core. This was also explained by Abanades [1] who stated that lime cannot completely carbonate to calcite due to internal sintering and decay in lime activity.

The final decrease in mass at 850-900 ^{0}C in the CaO TGA curve is related to the calcination of the produced $CaCO_3$ back to CaO.

To confirm the identification of hydrated lime $Ca(OH)_2$ in the sample, TGA for pure $Ca(OH)_2$ was also performed. In a nitrogen atmosphere, the TGA showed a mass drop to 77 % in the 400-600 ^{0}C temperature range, a value slightly higher than the theoretical value of 75 %. The mass drop in N_2 atmosphere is explained by the decomposition of $Ca(OH)_2$ (74 g/mol) to CaO (56 g/mol) and H_2O, resulting in 56/74= 75 % final mass. However, in CO_2 atmosphere, its behavior was different in that an increase in mass occurred to reach 131 %, that was followed by a mass drop to 73 %. The increase of mass in CO_2 atmosphere was explained by the fact that $Ca(OH)_2$ was transformed to $CaCO_3$ by two steps: first dehydration of $Ca(OH)_2$ to CaO followed rapidly by carbonation to $CaCO_3$. The mass increase was close to the theoretical amount of 135 % (equal to 100 g/mol $CaCO_3$ divided by 74 g/mol $Ca(OH)_2$). The mass drop that followed was due to calcite decomposition peaking at 875 ^{0}C and producing CaO. The final mass was lower than 100 % of the initial sample mass since the final product CaO (56 g/mol) has a lower molar mass than the initial component $Ca(OH)_2$ (74 g/mol). Note that the mass drop at 975 ^{0}C reached a value 2 % lower than the theoretical value of 75 % (equal 56 g/mol CaO divided by 74 g/mol $Ca(OH)_2$).

This slight error suggests that there may have been some $CaCO_3$ in the initial sample. The presence of small amount of $CaCO_3$ was also suggested by the small drop of mass in the 600-700 ^{0}C temperature range, from 77 to 75 % under N_2 atmosphere. A summary of the mass change for the different components is shown in Table 4.2, with indication of the temperature at which the peak change in mass occurs.

Table 4.2: Mass Change in TGA for different compounds and the Corresponding Peak Temperature in N_2 and CO_2 environment.

Gas	**S**	**CaO**	**$CaCO_3$**	**$Ca(OH)_2$**	**$CaSO_4$**
N_2	- 100 %	- 0 %	- 44 %	- 25 %	- 0 %
	at 300 °C	N/A	at 730 °C	at 440 °C	N/A
CO_2	- 100 %	+ 68 %	- 44 %	+ 31 %	- 0 %
	at 305 °C	at 600 °C	at 875 °C	at 475 °C	N/A

4.6.2 TGA for Product Samples

Once the thermal behavior of the pure components was understood, TGA tests for the product samples were performed. An example of a TGA run on one of the samples is shown in Figure 4.11, corresponding to the experiment where 1.0 gram of calcite was reacted with 0.16 g of sulfur, heated to 800 ^{0}C, in oxygen atmosphere.

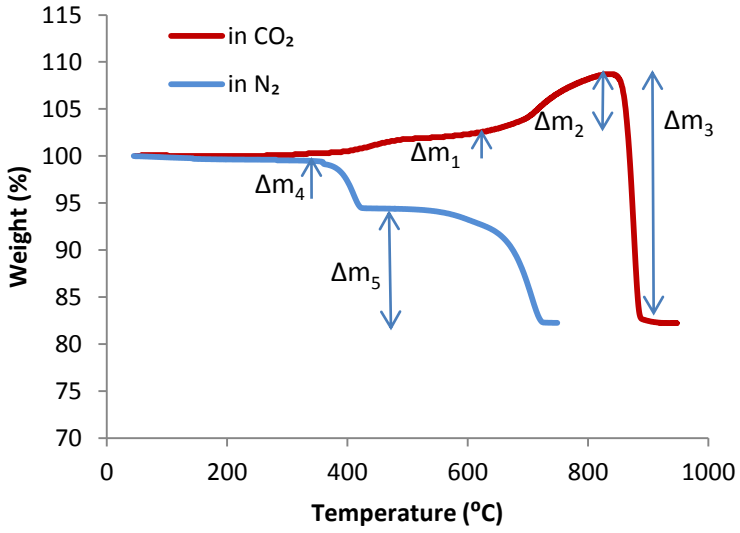

Figure 4.11: TGA for one the sample of 2:1 calcite to sulfur ratio heated to 800 ^{0}C under O_2 environment. Where Δm are the different mass changes that occurred in N_2 and CO_2 atmosphere.

In the TGA run under N_2 atmosphere, a mass drop first occurred in the 400-600 ^{0}C range followed by another drop between 600 and 750 ^{0}C. Based on the thermal analysis of various reactants in the previous section, it was concluded that the first mass drop Δm_4 in N_2 atmosphere was due to the presence of $Ca(OH)_2$, while Δm_5 corresponded to the presence of $CaCO_3$. TGA in CO_2 atmosphere was required to test for CaO, as it is thermally stable in N_2 atmosphere. The test showed an increase in mass Δm_1 of 3 % in the 400-600 ^{0}C range followed by another increase Δm_2 to 108 % in the 600 to 800 ^{0}C range. At 830 ^{0}C, the mass dropped suddenly until it reached 82 % at 900 ^{0}C. It was concluded that the first increase in mass Δm_1 was due to conversion of $Ca(OH)_2$ to $CaCO_3$. The second increase Δm_2 corresponded to the presence of CaO that carbonates to $CaCO_3$ at the higher temperature. The decrease in mass Δm_3 that started at 830 ^{0}C

was related to $CaCO_3$ that was formed from carbonation of $Ca(OH)_2$ and CaO, in addition to the $CaCO_3$ initially present in the sample.

For the remainder of the experiments, all of the samples were tested under CO_2 atmosphere. The presence of $Ca(OH)_2$, CaO and $CaCO_3$ in the samples was investigated by analysis of the mass change that occurred in TGA and by comparing them to the values shown in Table 4.2 for the pure components. No drop in mass related to sulfur was found in any of the samples.

The masses of $Ca(OH)_2$, CaO and $CaCO_3$ were calculated as follows with m being the measured mass (%) and M being the molar mass (g/mol); Δm_1 is the first mass increase between 400 and 600 ^{0}C, Δm_2 is the second mass increase between 600 and 800 ^{0}C, and Δm_3 is the mass decrease between 800 and 900 ^{0}C. The mass of CaO was corrected by a factor of 0.9 due to the fact that recarbonation capacity of CaO is 90 %. The Δm_3 corresponded to the total amount of $CaCO_3$; therefore to calculate for the initial mass of $CaCO_3$, the mass of $CaCO_3$ produced from CaO and $Ca(OH)_2$ was deducted.

- $m\,(Ca(OH)_2) = \Delta m_1 * \frac{M\,(Ca(OH)_2)}{M(CaCO_3) - M\,(Ca(OH)_2)}$

- $m\,(CaO) = \Delta m_2 * \frac{M(CaO)}{M(CO_2)} \div 0.9$

- $m\,(CaCO_3) = \left(\frac{\Delta m_3}{M(CO_2)} - \left[\frac{m\,(Ca(OH)_2)}{M\,(Ca(OH)_2)} + \frac{m\,(CaO)}{M(CaO)}\right]\right) * M(CaCO_3)$

Once the masses of $CaCO_3$, CaO and $Ca(OH)_2$ were calculated, the mass of $CaSO_4$ was calculated from:

- $m\,(CaSO_4) = 100\,\% - m\,(CaCO_3) + m(CaO) + m\,(Ca(OH)_2)$

The mass percentages were then converted to molar percentages so that the conversion of calcite to anhydrite could be computed. For samples with equimolar ratio of calcite to sulfur, and ratios of sulfur to calcite of 2:1 and 3:1, calcite was assumed to be the limiting reactant and the conversion is calculated based on its initial mass of 100 %. For samples where sulfur is half the molar amount of calcite, sulfur was assumed to be the limiting reactant and the corresponding initial mass of $CaCO_3$ expected to be converted is only its half.

For 1:1, 2:1 and 3:1 molar ratio, conversion X was computed from:

$$X = \frac{m\ (CaSO_4)}{M\ (CaSO_4)} \div \frac{m_{initial}\ (CaCO_3)}{M(CaCO_3)}$$

For 0.5:1 molar ratio, conversion X was computed from:

$$X = \frac{m\ (CaSO_4)}{M\ (CaSO_4)} \div 1/2\frac{m_{initial}\ \ (CaCO_3)}{M(CaCO_3)}$$

The results of conversion of calcite to anhydrite are shown in Table 4.3

Table 4.3: Conversion in one chamber reactor experiments as determined by quantitative analysis of TGA results, in function of Temperature, S-$CaCO_3$ ratio and Gas Flowed.

Reactant Ratio	**3:1**		**2:1**		**1:1**		**0.5:1**	
Temperature (^oC)	**O_2**	**Air**	**O_2**	**Air**	**O_2**	**Air**	**O_2**	**Air**
600	0.59	0.59	0.50	0.32	0.29	0.30	0.28	0.30
700	0.92	0.934	0.95	0.37	0.30	0.24	0.40	0.32
800	0.86	0.53	0.70	0.31	0.49	0.26	0.72	0.32
900	0.97	0.36	0.75	0.56	0.68	0.64	0.60	0.44

4.7 Results and Analysis from TGA and XRD Experiments

The results of conversion were assembled as a function of sulfur to calcite ratio for the four different temperatures, in air and oxygen atmospheres. These results were the average of results found from TGA experiments and XRD tests. Figure 4.12 shows the results at 600 ^{0}C. At 600 ^{0}C, the conversion from calcite to anhydrite was in clear dependence of the sulfur to calcite ratio. For example, in oxygen atmosphere, the conversion tested by TGA was 0.2 for S-$CaCO_3$ ratio of 0.5. Conversion increased in function of the ratio until it reached 0.65 for S-$CaCO_3$ ratio of 3. At 600 ^{0}C, the conversion in function of reactant ratio was found to be similar between the air and

oxygen atmospheres, except for a slightly lower conversion of 0.34 for the air atmosphere compared to 0.49 in O_2 for S-$CaCO_3$ ratio of 2.

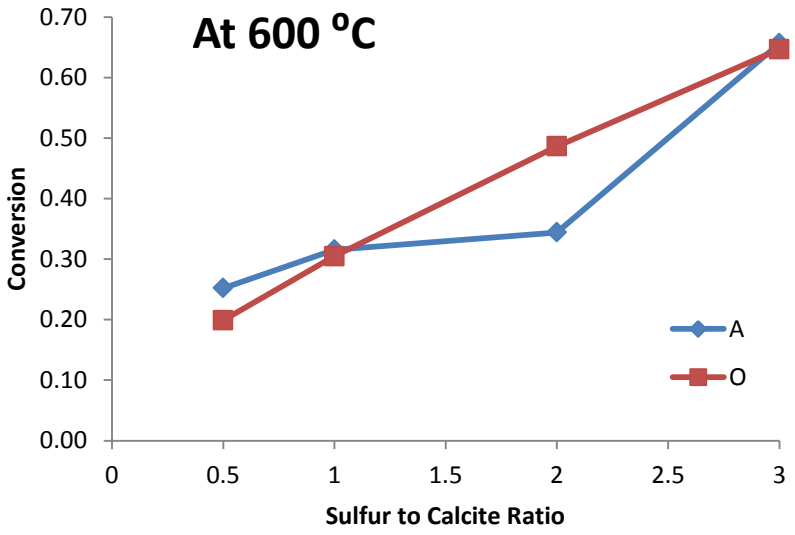

Figure 4.12: Conversion in function of S-$CaCO_3$ ratio at 600 ^{0}C, in oxygen and air atmospheres.

In Figure 4.13, the conversion results at 700 ^{0}C are shown.

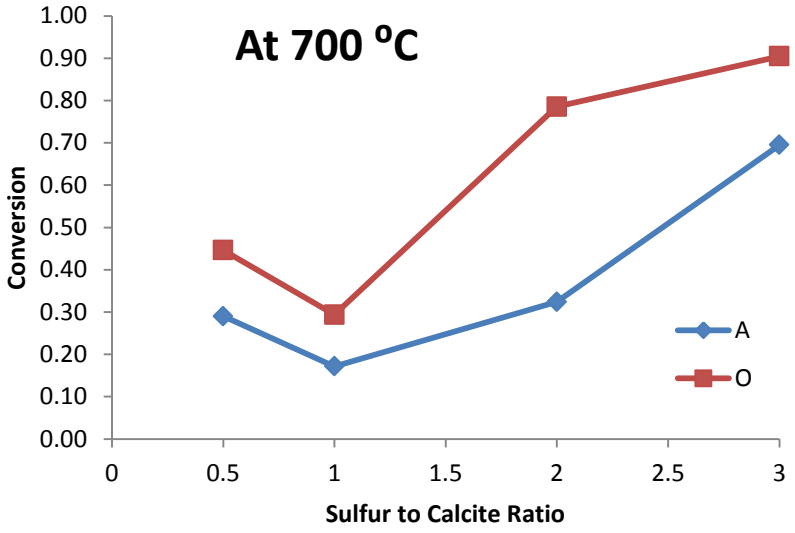

Figure 4.13: Conversion in function of S-$CaCO_3$ ratio at 700 ^{0}C, in oxygen and air atmospheres.

At 700 ^{0}C, the conversion trend in function of the ratio was slightly different than that at 600 ^{0}C; the conversion decreased from 0.45 to 0.29 between the 0.5 and 1 S-$CaCO_3$ ratio but then increased to 0.79 and 0.90 at 2 and 3 S-$CaCO_3$ ratios, in oxygen atmosphere.

In the air atmosphere tests, the conversion similarly decreased between the 0.5 and 1 S-$CaCO_3$ ratio from 0.29 to 0.17, and then increased to 0.32 and 0.69 at 2 and 3 S-$CaCO_3$ ratios.

The conversion showed an overall higher conversion compared to the experiments at 600 ^{0}C, due to the higher kinetics achieved at this temperature. However, conversion was shown to be higher in oxygen atmosphere compared to air, unlike the experiments at 600 ^{0}C that showed similarity between the two atmospheres. The higher conversion in pure O_2 gas was expected as it meant higher concentration of the oxygen reactant, compared to the air flow containing only 20 % O_2.

In Figure 4.14, the conversion results at 800 ^{0}C are shown.

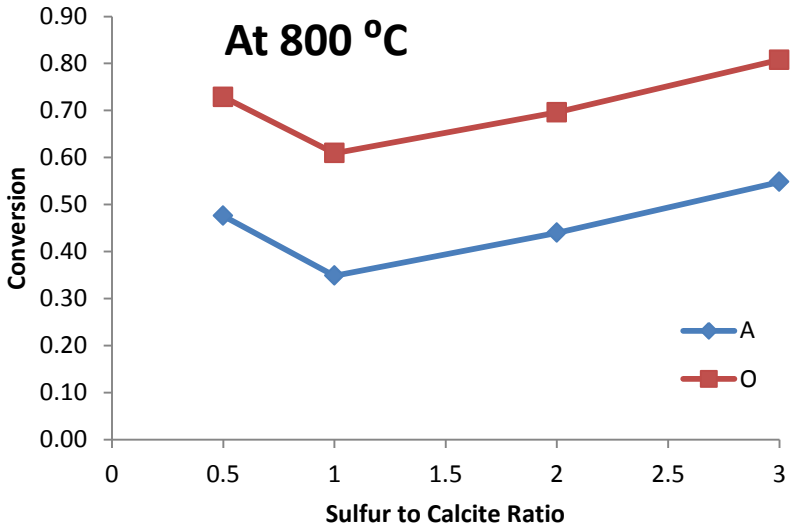

Figure 4.14: Conversion in function of S-$CaCO_3$ ratio at 800 ^{0}C, in oxygen and air atmospheres.

At 800 ^{0}C, the conversion was higher for S-$CaCO_3$ ratios of 0.5 and 1, in comparison with the respective values at 700 °C, by around 0.3 in O_2 atmosphere. The lowest conversion was 0.61 in oxygen atmosphere at S-$CaCO_3$ ratio of 1, and 0.74 for the ratio of 0.5. However, the values of conversion at S-$CaCO_3$ ratio of 2 and 3 were 0.70 and 0.81 respectively, values lower by 0.1 to respective values at 700 ^{0}C.

In air atmosphere, conversions were lower than the respective values in O_2 atmosphere, by 0.25, due to the lower oxygen concentration. From another side, conversion for 0.5, 1 S-$CaCO_3$ ratios were higher than those at 700 ^{0}C, by at least 0.18. At S-$CaCO_3$ ratio of 2, the value was higher than the respective value at 700 ^{0}C by 0.12, but lower by 0.15 at the S-$CaCO_3$ ratio of 3, showing that the excess ratio of sulfur to calcite resulted in a higher conversion at the lower temperature of 700 °C.

In Figure 4.15, the conversion results at 900 ^{0}C are shown.

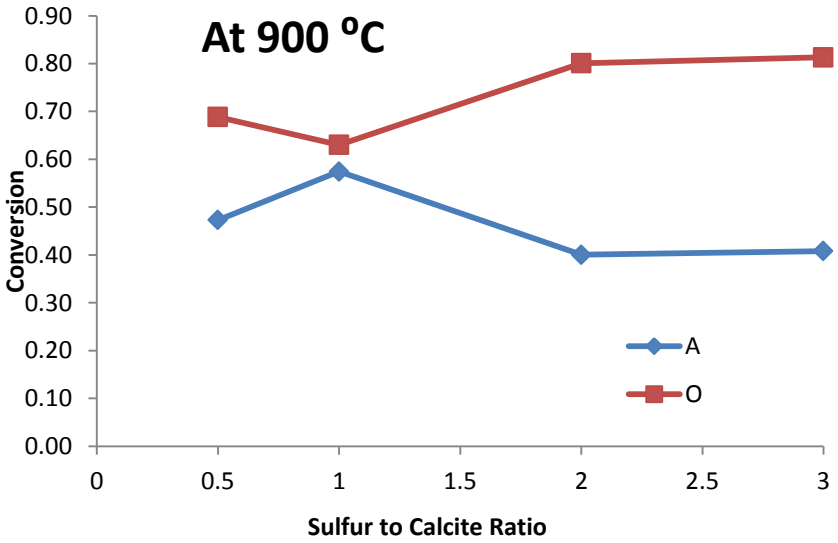

Figure 4.15: Conversion in function of S-$CaCO_3$ ratio at 900 ^{0}C, in oxygen and air atmospheres.

At 900 ^{0}C, the conversion at 0.5 and 1 S-$CaCO_3$ ratio were very similar to those achieved at 800 ^{0}C, being 0.04 smaller at S-$CaCO_3$ ratio of 0.5 and 0.02 higher at S-$CaCO_3$ ratio of 1. The conversion was 0.10 higher at S-$CaCO_3$ ratio of 2 but the same at the ratio of 3. This have suggested that the increase in kinetics of reaction due to increase in temperature between 800 and 900 ^{0}C was counter effected by the sintering effect of increasing temperature; therefore the conversions were close in value in O_2 atmosphere.

Conversion in air atmosphere showed the same conversion at S-$CaCO_3$ ratio of 0.5 between 800 and 900 °C and an increased conversion by 0.22 at S-$CaCO_3$ ratio of 1. However, conversion dropped at the higher ratios, being always lower than that in O_2. This decrease shows that despite the fact that sulfur is in excess, sintering effect increased and prevented the high conversion, since oxygen percentage was lower.

In summary, the conversion increased in function of temperature for S-$CaCO_3$ ratios of 0.5 and 1. The increase in temperature between 700 and 800 ^{0}C resulted in the biggest increase in conversion due to the change in calcination condition from uncalcined to calcined $CaCO_3$. The conversions at 800 and 900 ^{0}C were similar in values since the conversion at 900 ^{0}C couldn't reach higher values due to the likely sintering effect that occurs at this high temperature.

At S-$CaCO_3$ ratios of 2, temperature showed a less pronounced effect on conversion due to the fact that sulfur was in excess compared to calcite; at the S-$CaCO_3$ ratio of 3, the conversion was very similar between the different temperatures due to the fact that sulfur was at much higher excess value than required for reaction.

Using pure oxygen flow resulted in almost always higher conversion that in air atmosphere due to the 5 times greater concentration of oxygen in the pure O_2 flow compared to in air atmosphere.

The fact that conversion of sulfur to anhydrite at S-$CaCO_3$ ratio of 0.5 was higher than that at the 1 S-$CaCO_3$ ratio, can be explained by the fact that the lower ratio of S-$CaCO_3$ makes the calcite amount available for sulfur in excess (specifically twice the amount), and thus providing higher surface area of available calcite for reaction with sulfur.

In conclusion, heating a sample at S-$CaCO_3$ ratio of 0.5 to a temperature between 800 and 900 ^{0}C under oxygen atmosphere would provide optimum conditions to convert sulfur to anhydrite at the highest percentage possible. Having calcite in excess gives a higher surface area for reaction; the temperature between 800 and 900 ^{0}C is high enough to allow high conversion and low enough to prevent sintering of the sample. Using pure oxygen atmosphere allows higher conversion than air, although this might not be feasible if the process was to be scaled up.

4.8 Additional Experiments Regarding Pressurization

In addition to the previous experiments, further modifications to the design were performed with purpose of achieving experiments in a sealed vessel. The stainless steel reactor with flanges or Swagelok® fittings leaks the gas from the top fitting due to repetitive opening of the fitting to insert the sample, and the use of high temperatures. To provide a seal, different washers and O-rings of various materials were tested for performance, when inserted in the flanges. The O-rings used were either rubber or Teflon. The sealing was easily achieved for at least 10 minutes with the various rings and washers, when reactor was at room temperature. For example, when using the rubber O-ring, pressure was maintained at its initial pressure for at least 10 min as shown in Figure 4.16.

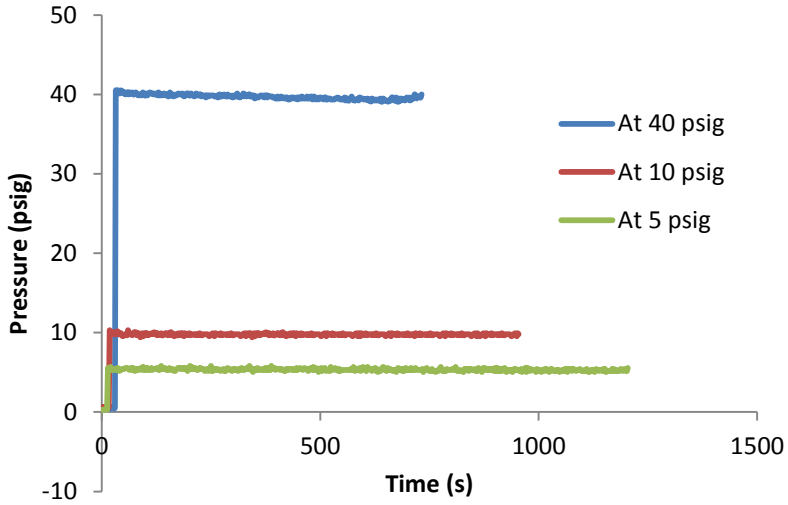

Figure 4.16: Pressure stability in function of time for a sealed reactor with rubber O-ring.

Then, the vessel was heated from room temperature to higher temperatures, with a starting pressure of 5 psig of air or nitrogen. Figure 4.17 showed an increase in the pressure with temperature; however, repeated experiments showed some variation in the maximum pressure reached for the same temperature. The challenge in increasing the pressure with temperature is in keeping the vessel sealed and preventing the leakage through the fitting. The increase in temperature at the flange level was deforming the O-rings made from Teflon or rubber; therefore, a gap between the flange and the ring was created and the gas inside the vessel was slightly escaping to the outside. The method that was followed to prevent the escape of gas was the continuous tightening of the bolts of the flange while the temperature increases and melts the ring.

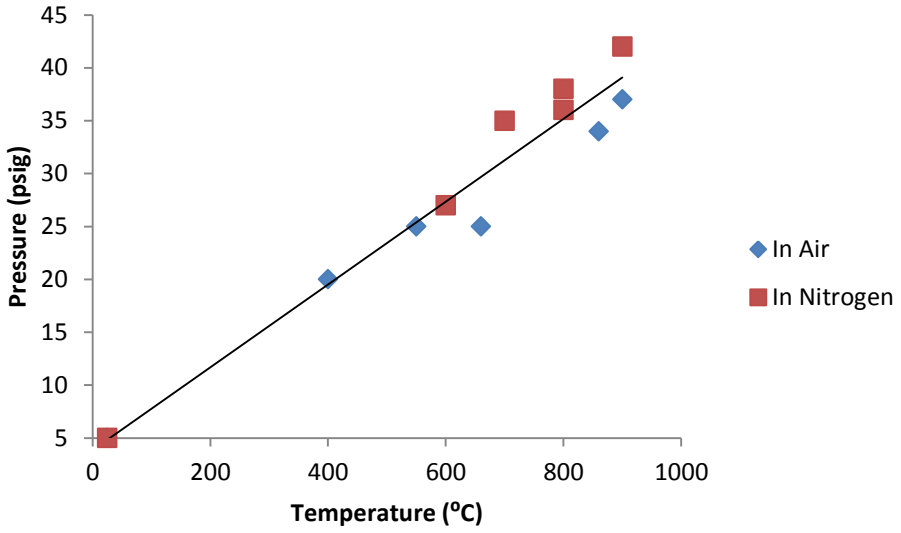

Figure 4.17: Maximum pressure reached in function of heating temperature achieved with rubber O-ring.

In addition, washers made of copper were also tested knowing that copper has a thermal expansion coefficient 1.03 times that of the stainless steel material of which the flange is made [2]. It was expected that the expansion of the washer would prevent the gap creation and the leakage; however, continuous tightening of the bolts was still necessary to prevent the leakage.

When continuous tightening was not performed, pressure would either not reach the expected value or decrease with time once the temperature was stabilized. Another approach to prevent the leakage was cooling down the fitting to prevent the expansion and thus the leakage. Dropping water on the flange was tried and resulted in good results of sealing; however, it was unsafe especially when working with a high temperature ceramic heater.

A suggested method is to substitute the reactor used with a longer one, such a way that the fitting would be far enough from the source of heat and therefore, no expansion at the fitting would occur.

In further experiments, the effect of adding a reactant in the vessel and the gasification of a product was shown to be noticeable. Figure 4.18 shows that when adding sulfur alone into the vessel, with 5 psig of nitrogen atmosphere, the pressure increased from 25 to 35 when 80 mg of S were added, and to 46 psig when sulfur amount was doubled. These values were reached at the temperature of 600 ^{0}C.

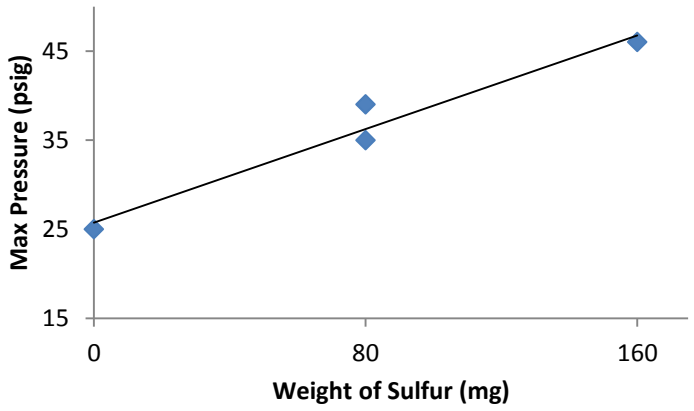

Figure 4.18: Pressure in function sulfur weight in vessel

Similarly, when adding 250 mg of $CaCO_3$, the maximum pressure reached at 900 ^{0}C increased from 42 to 69 psig, under nitrogen atmosphere, due to the emission of CO_2 from $CaCO_3$ calcination.

4.9 Summary and Conclusions

In summary, a series of lab-scale experiments was performed to better understand the factors that influence the reaction of calcite with sulfur and oxygen. Experiments started in a TGA apparatus where calcite and sulfur were mixed together in the sample pan, which was subjected to different gas conditions and a range of temperatures. The tests showed that the sulfur gasified and left the TGA furnace before any effective reaction with calcite. To ensure a longer contact time between

sulfur and calcite, two lab-scale apparatuses were constructed to perform additional tests. The first apparatus consisted of two heated vessels where the sulfur was inserted in an evaporator and the calcite was inserted in a downstream reactor. Once the sulfur was gasified, it flowed to the calcite reactor to form anhydrite. EDS tests confirmed the success of anhydrite formation in the experiments. However, sulfur was found to condense in the tube connecting the evaporator to the reactor and a new apparatus was designed to address this problem. In the new design, sulfur was inserted at the bottom part of the reactor vessel while calcite was kept in the middle, allowing upstream flow of sulfur to the level of the calcite. Experiments run in this apparatus involved changing the sulfur to calcite ratio, the temperature of reaction and the gas composition. TGA and XRD tests showed a general increase in the conversion as a function of temperature for 0.5:1 and 1:1 S-$CaCO_3$ ratios, being close in value at 800 and 900 °C. In addition, they showed a higher conversion for tests run under oxygen atmosphere compared to air. Tests performed with excess sulfur resulted in higher conversion of calcite, but lower than 100 %. In future, some replicate experiments should be performed to confirm the reproducibility of the experimental results. Also, the influence of oxygen partial pressure should be studied more carefully in a leakage-free vessel.

Future experiments should be conducted using limestone rather than pure $CaCO_3$, as it is widely available in nature and cheaper to use at a large-scale production. If $CaSO_4$ is to be a saleable product, then the resulting purity will also need to be studied. For future work, pilot plant should be also built where a continuous flow of reactants is introduced as to mimic an industrial scale process.

Based on this chapter that showed that the reaction of calcite, sulfur and oxygen can occur in the same vessel, future work should include modeling a large scale process similar to that studied in

Chapter 3; instead of a design where sulfur is oxidized then sent to a dry FGD system, sulfur and calcite can be introduced into the same boiler to produce heat that can be recovered in one unit.

4.10 Acknowledgements

Many thanks for Clarence McEwen, Brent Ball and Tim Nash for their technical help with designing and building the lab-scale apparatus. This work was funded by the Natural Sciences and Engineering Research Council of Canada (NSERC) through grant number 424223-2011.

4.11 References for Chapter 4

[1] Abanades JC. The maximum capture efficiency of CO2 using acarbonation/calcination cycle of CaO/CaCO3. Chemical Engineering Journal 90 (2002) 303–306.

[2] Haynes WM, Lide DR, D. R. CRC handbook of chemistry and physics: A ready-reference book of chemical and physical data- Chapter: Standard thermodynamic properties of chemical substances. Boca Raton, Fla.

Chapter 5

Conclusions and Recommendations

The main contribution of this thesis is the proposal and preliminary investigation of a promising route for conversion of elemental sulfur waste accumulated in stockpiles to an environmentally benign form, while producing reduced carbon electricity. The proposed route advances the zero-waste concept where all by-products of industrial processes are converted to their thermodynamic ground-state. This work is especially relevant as the world turns to "sour" fuels such as the oil sands of Alberta, which encouraged investigating into the potential for conversion of S to $CaSO_4$ and electrical power. This analysis is conducted via a thermodynamic model and laboratory-scale experiments.

Chapter 2 reviewed scientific literature on the life cycle of sulfur, its removal from petroleum products through Claus process, and its stockpiling in elemental form. There is a considerable literature on Flue Gas Desulfurization (FGD) systems for removal of SO_2 from flue gas in coal combustion and the effects of key operating parameters on $CaSO_4$ production are known from a variety of laboratory experiments. However, to the author's knowledge, conversion of excess S to $CaSO_4$ and electrical energy had not been studied until now.

In Chapter 3, a model-based study compared three possible systems for electricity production from sulfur using a natural gas combined cycle system as a reference case. In all three cases, the sulfur combustion unit and gas compressor/turbine system were combined with a FGD unit and a heat-recovery steam-generator (HRSG) system. The following conclusions were drawn from this study:

C3.1. The first case considered had relatively low efficiency because it does not permit energy recovery from exothermic SO_2 conversion to anhydrite in the FGD unit.

C3.2. The latter cases (Case 2a and Case 2b), obtain improved performance by placing the FGD unit upstream of the HRSG so that additional energy recovery can occur. Case 2b is more efficient than Case 2a because the gas turbine outlet temperature was lowered and therefore more energy was recovered by the gas turbine.

C3.3. The CO_2 emissions from Case 2b are the lowest among the SCC cases considered. Although the CO_2 emissions are higher than a comparable NGCC plant, they are lower than a new PC coal plant.

The preliminary analysis in Chapter 3 is a step toward a longer-term goal of converting waste sulfur to benign anhydrite and electrical energy with low CO_2 emissions. Several recommendations were made based on the results obtained in this chapter.

R3.1. Future process design and optimization studies should be performed to determine whether increased efficiency of power production and reduced CO_2 emissions can be obtained in practice compared to the values presented in this chapter.

R3.2. Further research is also required to obtain improved knowledge about any impediments (e.g., construction materials, reaction kinetics and achievable SO_2 emissions) to practical operation of this type of SCC system.

R3.3. Criteria such as capital cost, hours of operation and the need for new technology development, which have been ignored in the current thesis, should be considered in future design and optimization studies.

In Chapter 4, a series of lab-scale experiments was performed to better understand the factors that influence the reaction of calcite with sulfur and oxygen. Experiments started in a TGA apparatus where limestone and sulfur were mixed together in the sample pan, which was subjected to different gas conditions and a range of temperatures. The following conclusion was drawn based on the TGA experiments:

C4.1. The tests showed that the sulfur was gasified and left the TGA apparatus before any significant reaction with calcite.

To ensure a longer contact time between sulfur and calcite, two lab-scale apparatuses were constructed to perform additional tests. The first apparatus consisted of two heated vessels where the sulfur was inserted in an evaporator and the calcite was inserted in a downstream reactor. Once the sulfur was gasified, it flowed to the calcite reactor to form anhydrite. The following conclusions were drawn based on the results of these experiments:

C4.2. EDS tests confirmed the success of anhydrite formation in the experiments.

C4.3. Sulfur was found to condense in the tube connecting the evaporator to the reactor, indicating that a revised apparatus should be designed to address this problem.

It was decided to move the sulfur into the calcite reactor, below the calcite level, allowing sulfur gasification and sulfation in the same vessel. Experimental runs in this improved apparatus involved changing the sulfur to calcite ratio, the temperature of reaction and the gas composition. The following conclusions were drawn based on the results of these experiments:

C4.4. TGA and XRD tests showed a general increase of the conversion of sulfur to anhydrite in function of increase of temperature from 600 to 800 ^{0}C due to the increase in calcination. At 900

^{0}C, sintering occurred resulting in a counter-effect of temperature increase and therefore the conversion at 900 ^{0}C was no greater than that at 800 ^{0}C.

C4.5. The TGA and XRD analyses also showed that at S-$CaCO_3$ ratio of 0.5, conversion of S to $CaSO_4$ was higher than when the reactants were at equimolar ratio; this was explained by the greater surface area of calcite provided for sulfur when the latter is at ratio of half. At high ratios of S-$CaCO_3$, sulfur was provided in excess and therefore higher sulfation conversion occurred. At high S-$CaCO_3$ ratios, the conversions were close in value for different temperatures, showing that at lower temperatures of 600 ^{0}C, high sulfation degree can occur due to the excess of sulfur.

C4.6. The results also showed that experimental runs under oxygen atmosphere resulted in higher conversions than in air atmosphere, due to the greater concentration of the reactant oxygen compared to that in air.

C4.7. The experimental results obtained in Chapter 4 confirmed that $CaSO_4$ can readily be produced from $CaCO_3$ and S during a short time period (< 1 minute). The best conditions for conversion found from the experiments performed are a temperature between 800 and 900 ^{0}C, in an oxygen environment, with a S-$CaCO_3$ ratio of 0.5.

The following recommendations arose from the experiments conducted in the revised reactor system:

R4.1. In future, variation of temperature between 800 and 900 ^{0}C should be performed to find the exact optimum temperature of reaction. Experiments at a S-$CaCO_3$ molar ratio of 0.25 and 0.75 should also be conducted to find the effect of varying the molar ratio in the lower range. More

replicate experiments should be performed to confirm the reproducibility of the experimental results.

R4.2. The influence of oxygen partial pressure should be studied more carefully in a sealed apparatus, to see the effect of pressurizing the reactants on the conversion.

R4.3. Future experiments should be conducted using limestone rather than pure $CaCO_3$ in the reactor knowing that limestone would be preferred to be used in large-scale production because it is widely available in nature.

R4.4. If future experimental results continue to show promise, a pilot-scale plant should be built where a continuous flow of reactants is introduced to better mimic the behavior of an industrial-scale process.

R4.6. Because the experiments in Chapter 4 showed that the reaction of calcite, sulfur and oxygen can readily occur in the same vessel, future work should include modeling of a large-scale process similar to that studied in Chapter 3, except that the process would be in a single boiler similar to that used in coal plants.

Appendix A

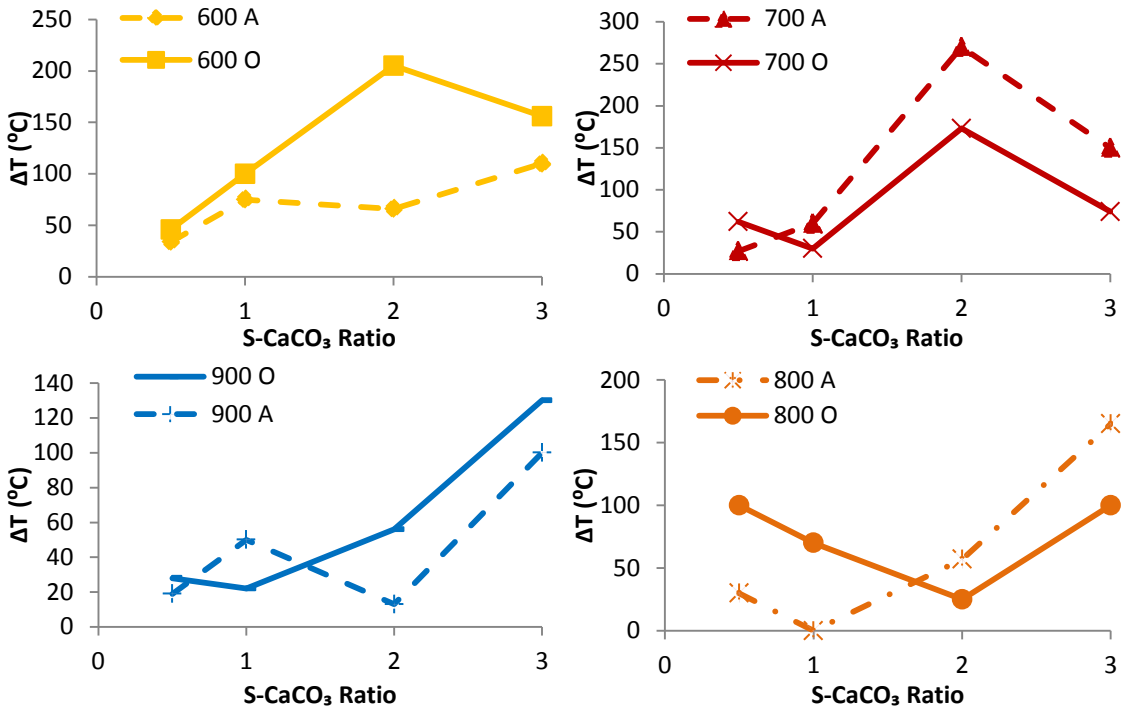

Figure A.1: Increase in temperature after flow of gas, in function of reactants ratio, for different temperatures**.**

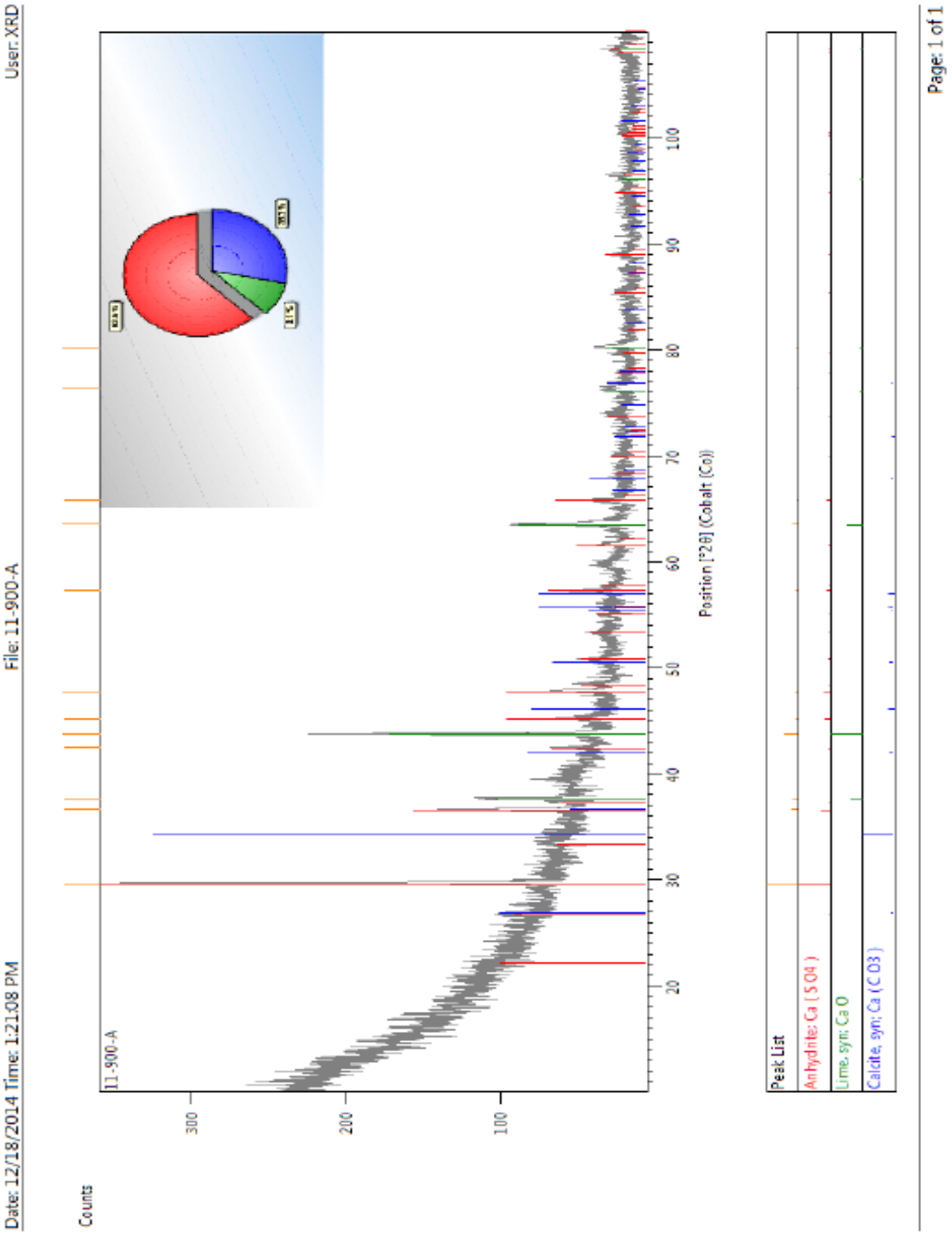

Figure A.2: Diffractogram Pattern of a sample example.

Table A.1: XRD responses for the 32 samples. Note: A is air and O is oxygen.

Temperature (^{0}C)	**Ratio**	**Gas**	$CaCO_3$ (%)	$CaSO_4$ (%)	CaO (%)	CaS (%)	S_8 (%)	$Ca(OH)_2$ (%)
600	**0.5**	**A**	71	14		15		
600	**1**	**A**	49	36	3		12	
600	**2**	**A**	47	40	2		10	
600	**3**	**A**	9	83	8			
600	**0.5**	**O**	79	7			13	
600	**1**	**O**	60	39	1			
600	**2**	**O**	35	50	3		12	
600	**3**	**O**	19	79	3			
700	**0.5**	**A**	79	17	1	3		
700	**1**	**A**	86	14	1			
700	**2**	**A**	56	36		8		
700	**3**	**A**	3	64	19	14		
700	**0.5**	**O**	58	32	3	7		
700	**1**	**O**	51	38	8	3		
700	**2**	**O**	6	74	2	17		
700	**3**	**O**	1	94	1	4		
800	**0.5**	**A**	51	41	8			
800	**1**	**A**	41	48	2		6	4
800	**2**	**A**	31	65	3			
800	**3**	**A**	5	73	16	6		
800	**0.5**	**O**	45	46	5	3		
800	**1**	**O**	16	73		3	8	
800	**2**	**O**	13	74	3	4	6	
800	**3**	**O**	7	84	2	7		
900	**0.5**	**A**	46	36	18			
900	**1**	**A**	28	62	9			
900	**2**	**A**	12	41	42	4		
900	**3**	**A**	7	65	28			
900	**0.5**	**O**	29	53	18			
900	**1**	**O**	20	69	1	11		
900	**2**	**O**	8	90	2			
900	**3**	**O**	18	75	2	5		